

Calibratable Disambiguation Loss for Multi-Instance Partial-Label Learning

Wei Tang, Yin-Fang Yang, Weijia Zhang, and Min-Ling Zhang, Senior Member, IEEE

Abstract—Multi-instance partial-label learning (MIPL) is a weakly supervised framework that extends the principles of multi-instance learning (MIL) and partial-label learning (PLL) to address the challenges of inexact supervision in both instance and label spaces. However, existing MIPL approaches often suffer from poor calibration, undermining classifier reliability. In this work, we propose a plug-and-play calibratable disambiguation loss (CDL) that simultaneously improves classification accuracy and calibration performance. The loss has two instantiations: the first one calibrates predictions based on probabilities from the candidate label set, while the second one integrates probabilities from both candidate and non-candidate label sets. The proposed CDL can be seamlessly incorporated into existing MIPL and PLL frameworks. We provide a theoretical analysis that establishes the lower bound and regularization properties of CDL, demonstrating its superiority over conventional disambiguation losses. Experimental results on benchmark and real-world datasets confirm that our CDL significantly enhances both classification and calibration performance.

Index Terms—Multi-instance partial-label learning, partial-label learning, disambiguation loss, model calibration.

1 INTRODUCTION

WEAKLY supervised learning enables the construction of predictive models with limited supervision. According to [1], weak supervision can be classified into three types: inexact, inaccurate, and incomplete. Inexact supervision arises from a coarse alignment between instances and labels, a common and challenging issue in real-world applications. Two prominent frameworks that address inexact supervision from different perspectives are *multi-instance learning (MIL)* [2], [3], [4], [5], [6], [7], [8], [9] and *partial-label learning (PLL)* [10], [11], [12], [13], [14], [15], [16], [17]. MIL addresses inexactness in the instance space, where the positive instances within a bag are unidentified, while PLL focuses on inexactness in the label space, where the true label remains hidden within a candidate label set.

Recent advancements have introduced *multi-instance partial-label learning (MIPL)* [19], which generalizes these frameworks to scenarios with dual inexact supervision, where both the instance space and the label space contain inexactness. In MIPL, each training sample consists of a multi-instance bag associated with a candidate label set that includes the true label and several false positive labels. During training, both the positive instances in the instance space and the true label in the label space remain unknown. Fig. 1 illustrates an application of MIPL in pathology image classification, where images are typically segmented into patches to manage computational demands [20]. To reduce annotation costs, labels are often obtained from crowd-sourced annotators instead of expert pathologists [18], [21]. However, due to their limited expertise in pathology, crowd-

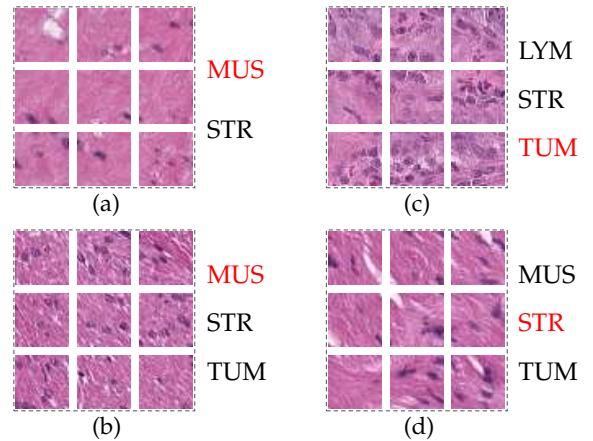


Fig. 1. Pathology image classification with crowd-sourced candidate label sets is a MIPL scenario [18], where true labels are highlighted in red and false positive labels in black. The labels include LYM (lymphocytes), MUS (smooth muscle), STR (cancer-associated stroma), and TUM (colorectal adenocarcinoma epithelium).

sourced annotators may struggle to accurately identify the true label. To address this challenge, providing a candidate label set for each image is a practical approach. Consequently, MIPL emerges as a natural framework to tackle this problem, as it is specifically designed to handle such dual inexact supervision in both instance and label spaces.

Existing MIPL approaches can be categorized into two paradigms: the instance-space paradigm and the embedded-space paradigm. The instance-space paradigm generates a predicted label for a multi-instance bag by aggregating the prediction probabilities of its constituent instances [19]. In contrast, the embedded-space paradigm classifies multi-instance bags directly by aggregating them into a single feature vector [18], [22], [23]. The latter paradigm often exhibits superior classification performance owing to its ability to capture global feature representations. A crucial

- Wei Tang, Yin-Fang Yang, and Min-Ling Zhang are with the School of Computer Science and Engineering, Southeast University, Nanjing 210096, China, and the Key Laboratory of Computer Network and Information Integration (Southeast University), MoE, China. E-mail: {tangw, yangyf, zhangml}@seu.edu.cn.
- Weijia Zhang is with the School of Information and Physical Sciences, The University of Newcastle, Callaghan, NSW 2308, Australia. E-mail: weijia.zhang@newcastle.edu.au.
- Corresponding author: Min-Ling Zhang.

aspect of MIPL training is label disambiguation, which involves identifying the true label from the candidate set and significantly influences classification performance [18], [24]. However, current MIPL approaches focus exclusively on disambiguation while neglecting model calibration, which undermines their applicability in scenarios where reliable confidence estimates are necessary for decision-making.

As illustrated in Fig. 2 (a), (b), and (c), the predicted confidences of DEMIPL [18], ELIMIPL [22], and MIPLMA [23] tend to cluster around 0.25, leading to poor calibration performance. This limitation diminishes their effectiveness in high-stakes applications. For example, in pathology image classification, accurate calibration is crucial for distinguishing between benign and malignant cell types in tissue samples. Reliable confidence scores are essential for guiding clinical decisions, enabling early diagnosis, and informing treatment planning. Poorly calibrated models may misrepresent predictive uncertainty, increasing the risk of misdiagnosis and suboptimal medical interventions.

To overcome these challenges, we propose a plug-and-play Calibratable Disambiguation Loss (CDL) that jointly addresses classification and calibration in MIPL methods. Specifically, CDL has two instantiations: the first considers the maximum and second-highest prediction probabilities among candidate labels, while the second contrasts the highest candidate-label probability with the highest probability of a non-candidate label. Moreover, our CDL can be seamlessly integrated into existing MIPL frameworks. As demonstrated in Fig. 2 (d)-(i), our methods employing CDL demonstrate improved classification accuracy and reduced expected calibration error, making them more reliable for assessing pathological slides.

Our key contributions are as follows: 1) To the best of our knowledge, this work is the first to address the calibration challenge in MIPL. 2) We provide theoretical insights that validate the lower bound and regularization properties of CDL. 3) Extensive experiments on benchmark and real-world datasets confirm that our CDL achieves state-of-the-art performance in both classification and calibration.

2 RELATED WORK

2.1 Multi-Instance Learning

Multi-instance learning (MIL), initially developed for drug activity prediction [25], has since been applied across diverse fields, including text classification [2], [3], [26], object detection [27], and video anomaly detection [28]. Recent advancements in MIL often incorporate attention mechanisms to synthesize features from multiple instances within a bag into a cohesive representation for classification. For example, Ilse *et al.* [4] introduced both plain and gated attention mechanisms, which significantly improved the performance of binary MIL tasks. An extension of this paradigm, the loss-based attention mechanism [29] effectively addresses multi-class classification challenges. The success of attention-based MIL approaches has led to their widespread adoption in applications such as pathology image classification [30], [31] and time series classification [32]. These approaches utilize a weighted aggregation of attention scores and instances to generate a comprehensive bag-level feature.

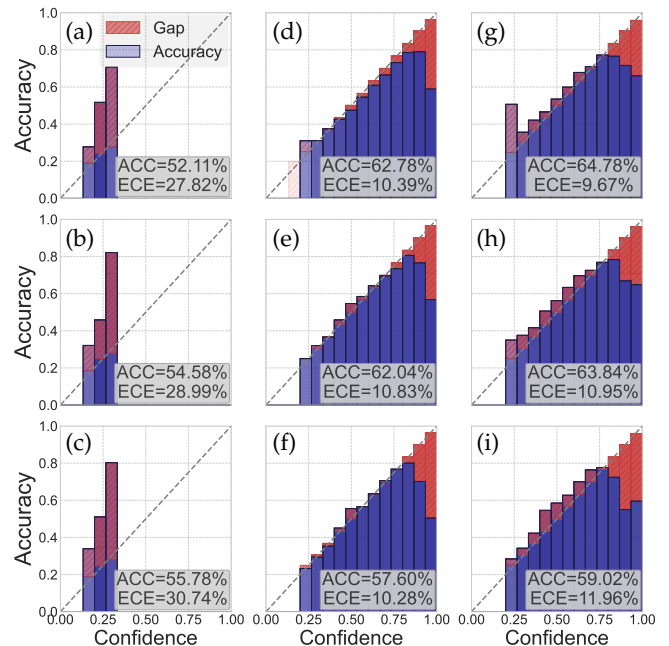


Fig. 2. Reliability diagrams of (a) DEMIPL [18], (b) ELIMIPL [22], (c) MIPLMA [23], (d) DAMCC, (e) SAMCC, (f) MAMCC, (g) DAMCN, (h) SAMCN, and (i) MAMCN on the C-KMeans test set. The diagrams display mean accuracy (ACC) and expected calibration error (ECE) from ten runs, with (d)-(i) representing our methods. The bar color intensity reflects the number of samples assigned to the corresponding confidence intervals.

Despite the significant advancements, existing MIL approaches remain ineffective for MIPL scenarios because they cannot directly handle ambiguous candidate label sets [19].

2.2 Partial-Label Learning

Partial-label learning (PLL) has diverse applications across numerous real-world domains, such as face naming [10], [33], [34], object classification [35], [36], bioinformatics [37], and facial age estimation [38], [39]. Recent developments have led to the emergence of several deep learning-based PLL methods. For example, Lv *et al.* [24] utilized linear classifiers and multi-layer perceptrons to generate feature representations from instances, employing progressive disambiguation techniques to identify the true labels. Building on this foundation, Feng *et al.* [40] explored the process of generating PLL data and introduced two theoretically robust algorithms for PLL. Similarly, Wen *et al.* [41] proposed a weighted loss function for disambiguation that provides a versatile approach applicable to various algorithms. Furthermore, Xu *et al.* [15] applied progressive purification of candidate labels to train classifiers within the instance-dependent PLL framework. Recently, Wang *et al.* [42] established the first PLL benchmark and introduced theoretically justified model selection criteria for PLL.

However, the inherent limitations of these PLL approaches in handling inexact supervision in the instance space impede their effectiveness in MIPL scenarios [19].

2.3 Multi-Instance Partial-Label Learning

Multi-instance partial-label learning (MIPL) extends MIL and PLL to address dual inexact supervision, where both

input instances and output labels are ambiguous. Tang *et al.* [19] introduced the MIPL framework alongside the MIPLGP algorithm, which follows an instance-space paradigm and consists of three key steps. First, it assumes all negative instances belong to a negative class and assigns a pseudo-negative class to each candidate label set. Next, it propagates bag-level candidate labels to individual instances. Finally, it introduces Dirichlet disambiguation and employs Gaussian process regression to resolve inexactness.

In contrast, DEMIPL [18] adopts an embedded-space paradigm, encoding multi-instance bags into compact representations via an attention mechanism, followed by a momentum-based strategy to identify true labels. Building upon the embedded-space paradigm, ELIMIPL [22], PROMIPL [43], and MIPLMA [23] integrate attention mechanisms with specialized disambiguation loss functions to learn bag-level representations and refine bag-level labels. Furthermore, Yang *et al.* [44] proposed a mixed-effects model to capture dependencies between instances and bags, significantly improving computational efficiency. Meanwhile, Wang *et al.* [45] explored MIPL in the context of latent structural learning and neuro-symbolic integration, broadening its applicability beyond conventional disambiguation.

Despite notable advancements, current MIPL approaches primarily focus on disambiguation, which remains an underexplored challenge in model calibration.

2.4 Model Calibration

Model calibration is crucial for ensuring that predicted probabilities accurately reflect true likelihoods of the respective classes [46]. Calibration methods can be broadly categorized into training-time and post-hoc approaches. Training-time calibration technologies incorporate regularization techniques during training to address overconfidence in deep neural networks. For example, label smoothing is a prominent technique that reduces overfitting and enhances calibration by mitigating excessively confident predictions [47], [48]. Implicit regularization methods, such as mixup training and focal loss, originally designed to improve generalization, have also proven effective for calibration [48], [49], [50], [51], [52]. The post-hoc calibration methods adjust model outputs after training to better align predicted probabilities with true likelihoods. Platt scaling refines binary classifier outputs using learned parameters [53], [54], whereas temperature scaling, an extension of Platt scaling, rescales logits in multi-class tasks using a learned temperature parameter [46].

While the above calibration techniques provide substantial benefits for supervised learning tasks, using them for MIPL is challenging due to the absence of true labels.

3 PRELIMINARIES

3.1 Notations

We formalize a MIPL training dataset as $\mathcal{D} = \{(\mathbf{X}_i, \mathcal{S}_i) \mid 1 \leq i \leq m\}$, where \mathcal{D} consists of m multi-instance bags, each associated with a corresponding candidate label set. The instance space is represented by $\mathcal{X} = \mathbb{R}^d$, and the label space is denoted as $\mathcal{Y} = \{1, 2, \dots, k\}$, which includes k distinct class labels. Specifically, the i -th multi-instance bag

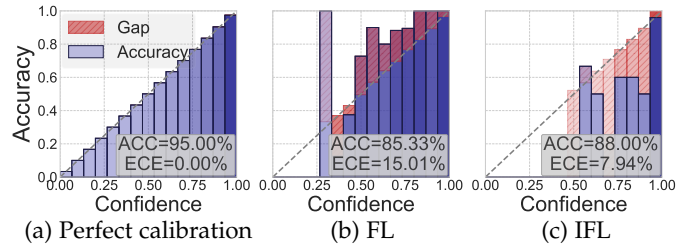


Fig. 3. Reliability diagrams of SAM [22] with FL or IFL on the FMNIST-MIPL dataset with one false positive label ($r = 1$).

$\mathbf{X}_i = \{x_{i,1}, x_{i,2}, \dots, x_{i,n_i}\}$ contains n_i instances within a d -dimensional space. The candidate label set \mathcal{S}_i and the non-candidate label set $\bar{\mathcal{S}}_i$ are subsets of \mathcal{Y} , satisfying the constraints $\mathcal{S}_i \cup \bar{\mathcal{S}}_i = \mathcal{Y}$ and $\mathcal{S}_i \cap \bar{\mathcal{S}}_i = \emptyset$.

Notably, each bag contains at least one instance corresponding to the true label: there exists $x_{ir} \in X_i$ such that $f(x_{ir}) = y \in \mathcal{Y}$, where y and f are the ground-truth and unknown labelling mechanism, respectively. Furthermore, each bag also excludes instances associated with the false positives, e.g., for any $x_{i,s} \in X_i$, $f(x_{i,s}) \notin \mathcal{Y}$. For example, in pathology image classification [18], positive instances represent specific cell types, such as lymphocytes or colorectal adenocarcinoma epithelium, whereas negative instances include background regions or non-cellular areas.

3.2 Calibration

A well-calibrated model ensures that the confidence scores of the predictions reflect the true probabilities of correctness [46], [52], [55], [56], which can be formally expressed as:

$$\mathbb{P}(\hat{y} = y \mid \hat{p} = p) = p, \quad \forall p \in [0, 1], \quad (1)$$

where \hat{y} and \hat{p} denote the predicted label and confidence score, respectively, while y represents the true label. The confidence score p is the model's estimated probability that the prediction \hat{y} is correct.

The expected calibration error (ECE) quantifies calibration quality from finite samples by partitioning the predicted confidences into R bins $\{B_r\}_{r=1}^R$ and computing:

$$\text{ECE} = \sum_{r=1}^R \frac{|B_r|}{m} |A_r - P_r|, \quad (2)$$

where $A_r = \frac{1}{|B_r|} \sum_{i \in B_r} \mathbb{I}(\hat{y}_i = y_i)$ and $P_r = \frac{1}{|B_r|} \sum_{i \in B_r} \hat{p}_i$ represent the accuracy and average confidence in bin r , respectively. This metric assesses how well-predicted confidences align with actual correctness, typically employing $R = 15$ bins. A model is well-calibrated if its predicted confidences closely reflect empirical accuracies. Fig. 3 (a) illustrates perfect calibration using generated data, where, in each bin, predicted confidences precisely match accuracies, resulting in perfect calibration, i.e., $\text{ECE} = 0$.

Focal loss (FL) [57] was introduced to mitigate class imbalance in object detection by reducing the loss weight for predicted samples with high confidence. Mukhoti *et al.* [51] demonstrated that replacing cross-entropy loss with FL enhances model calibration. Moreover, Wang *et al.* [48] proposed inverse focal loss (IFL), which improves calibration performance further. The formulations of FL and IFL are:

$$\mathcal{L}_{\text{FL}} = -(1 - \hat{p}_{i,y_i})^\gamma \log \hat{p}_{i,y_i}, \quad (3)$$

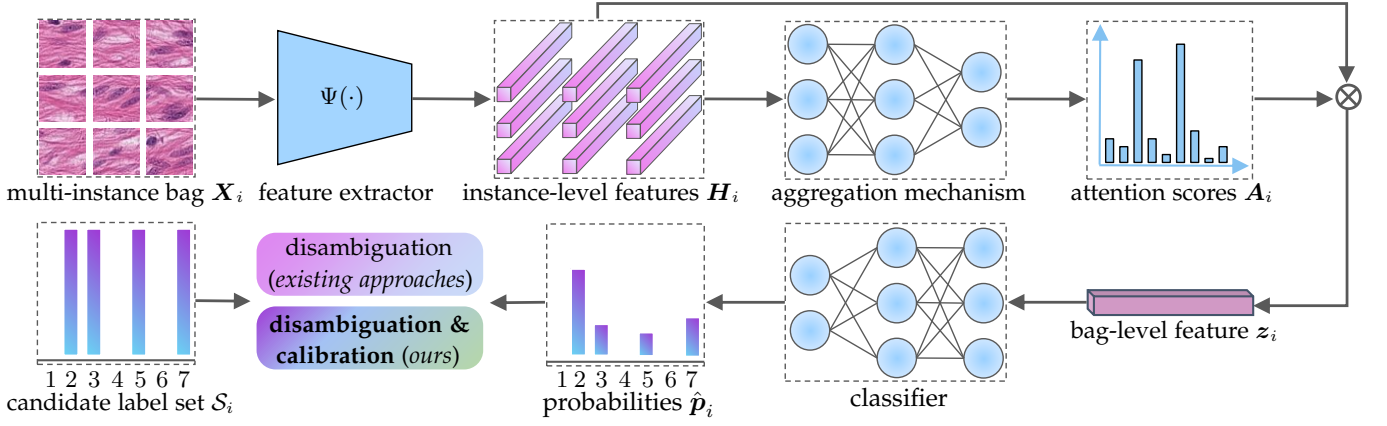


Fig. 4. Framework of MIPL approaches within the embedded-space paradigm.

$$\mathcal{L}_{\text{IFL}} = -(1 + \hat{p}_{i,y_i})^\gamma \log \hat{p}_{i,y_i}, \quad (4)$$

where y_i denotes the true label of the i -th sample.

In standard supervised learning, focal losses significantly improve calibration. However, applying FL and IFL in MIPL is challenging due to the absence of true labels, as illustrated in Fig. 3 (b) and (c).

3.3 The Pitfalls of Naive Focal Losses in MIPL

One native approach for extending the focal losses to MIPL is to select the candidate label with the highest predicted probability as a surrogate of the true label. However, this naive implementation does not create well-calibrated models and also significantly reduces the classification accuracy in MIPL. To compensate for this, we propose to employ all candidate labels with different weights. Specifically, we utilize the Scaled additive Attention Mechanism (SAM) in ELIMIPL [22] to derive the holistic features of multi-instance bags, coupled with FL or IFL as the loss function. Since FL and IFL were originally designed for fully supervised settings, we refine FL and IFL for MIPL as follows:

$$\mathcal{L}_{\text{FL}}^{\text{MIPL}} = - \sum_{c \in S_i} w_{i,c}^{(t)} (1 - \hat{p}_{i,c}^{(t)})^\gamma \log(\hat{p}_{i,c}^{(t)}), \quad (5)$$

$$\mathcal{L}_{\text{IFL}}^{\text{MIPL}} = - \sum_{c \in S_i} w_{i,c}^{(t)} (1 + \hat{p}_{i,c}^{(t)})^\gamma \log(\hat{p}_{i,c}^{(t)}), \quad (6)$$

where S_i is the candidate label set of the i -th multi-instance bag and $\hat{p}_{i,c}$ is the predicted probabilities on the c -th label. $w_{i,c}^{(t)}$ denotes the weights of the c -th class at the t -th epoch.

Experimental results in Fig. 3 reveal that the average classification accuracy using FL and IFL for calibration is lower compared to that of ELIMIPL (90.27%). Specifically, FL suffers from under-confidence, where classification accuracy significantly exceeds predicted confidence, while IFL exhibits over-confidence, where predicted confidence significantly surpasses classification accuracy. The results indicate that while FL and IFL can be adapted for MIPL, their effectiveness is constrained, resulting in reduced classification accuracy and notable under-confidence and over-confidence issues. Thus, despite their strong performance in standard supervised learning, applying FL and IFL in MIPL requires further refinement and optimization.

4 THE PROPOSED APPROACH

The framework of the MIPL approaches based on the embedded-space paradigm is detailed in Fig. 4. First, a feature extractor $\Psi(\cdot)$ generates instance-level feature representations H_i from the i -th multi-instance bag X_i . Second, an aggregation mechanism combines H_i into a unified feature vector z_i . Subsequently, a classifier estimates the probability distribution \hat{p}_i for each multi-instance bag. Unlike the existing MIPL methods that focus solely on disambiguation, our approach integrates an additional emphasis on model calibration, thereby providing a more comprehensive solution.

4.1 Aggregation Mechanisms in MIPL

In MIPL, aggregation mechanisms play a crucial role in integrating information from multi-instance bags. Given a multi-instance bag $X_i = \{\mathbf{x}_{i,1}, \mathbf{x}_{i,2}, \dots, \mathbf{x}_{i,n_i}\}$, its instance-level feature representations $H_i = \Psi(X_i) = \{\mathbf{h}_{i,1}, \mathbf{h}_{i,2}, \dots, \mathbf{h}_{i,n_i}\}$ are learned via a feature extractor $\Psi(\cdot)$. The significance of the j -th instance within the i -th multi-instance bag is modeled as follows:

$$\xi(h_{i,j}) = \mathbf{W}^\top (\tanh(\mathbf{W}_t^\top \mathbf{h}_{i,j}) \odot \text{sigm}(\mathbf{W}_s^\top \mathbf{h}_{i,j})), \quad (7)$$

where \mathbf{W}^\top , \mathbf{W}_t^\top , and \mathbf{W}_s^\top are learnable weight matrices, including bias terms. Here, $\tanh(\cdot)$ and $\text{sigm}(\cdot)$ denote the hyperbolic tangent and sigmoid functions, respectively, and \odot represents element-wise multiplication.

The central aspect of aggregation mechanisms is the computation of attention scores. Existing aggregation mechanisms in MIPL can be categorized into three types: Disambiguation Attention Mechanism (DAM) in DEMIPL [18], Scaled additive Attention Mechanism (SAM) in ELIMIPL [22], and Margin-aware Attention Mechanism (MAM) in MIPLMA [23] and PROMIPL [43]. While all three mechanisms employ attention mechanisms for aggregation, they differ in how attention scores are computed.

- 1) DAM determines the attention scores by applying a nonlinear transformation to $\xi(h_{i,j})$:

$$a_{i,j} = \frac{1/\{1 + \exp\{-\xi(h_{i,j})\}\}}{\sum_{j'=1}^{n_i} 1/\{1 + \exp\{-\xi(h_{i,j'})\}\}}. \quad (8)$$

- 2) SAM refines attention scores by exponentiating $\xi(h_{i,j})$ and introducing a scaling factor l :

$$a_{i,j} = \frac{\exp\{\xi(h_{i,j})/\sqrt{l}\}}{\sum_{j'=1}^{n_i} \exp\{\xi(h_{i,j'})/\sqrt{l}\}}. \quad (9)$$

- 3) MAM dynamically adjusts attention scores during training by varying the temperature parameter $\tau^{(t)}$:

$$\check{a}_{i,j} = \frac{\exp\{\xi(h_{i,j})/\tau^{(t)}\}}{\sum_{j'=1}^{n_i} \exp\{\xi(h_{i,j'})/\tau^{(t)}\}}. \quad (10)$$

At the first epoch, the temperature parameter is initialized as a predefined constant and is annealed at the t -th epoch according to:

$$\tau^{(t)} = \max\{\tau_m, \tau^{(t-1)} * 0.95\}, \quad (11)$$

where τ_m denotes the minimum temperature parameter, and $\tau^{(0)}$ is the predefined initial value. To stabilize training, a normalization operation is applied to the attention scores $\check{a}_{i,j}$:

$$a_{i,j} = \frac{\check{a}_{i,j} - \bar{a}_i}{\sqrt{\sum_{j'=1}^{n_i} (\check{a}_{i,j'} - \bar{a}_i)^2 / (n_i - 1)}}, \quad (12)$$

where $\bar{a}_i = \frac{1}{n_i} \sum_{j'=1}^{n_i} \check{a}_{i,j'}$ represents the mean attention score for the i -th multi-instance bag.

After computing attention scores using one of the three mechanisms, the bag-level feature \mathbf{z}_i is obtained as a weighted sum of the scores and instance-level features:

$$\mathbf{z}_i = \sum_{j=1}^{n_i} a_{i,j} \mathbf{h}_{i,j}. \quad (13)$$

In summary, all three MIPL attention mechanisms have the same workflow but differ in their computation of the attention scores.

4.2 Calibratable Disambiguation Loss

As illustrated in Fig. 3, applying FL and IFL to MIPL can lead to under-confidence and over-confidence in the predicted probabilities. To tackle these problems, we introduce a novel calibratable disambiguation loss (CDL) specifically designed to balance prediction probabilities.

Definition 1 (Calibratable Disambiguation Loss). *The Calibratable Disambiguation Loss (CDL) for multi-instance partial-label learning is defined as:*

$$\mathcal{L}_{CDL} = - \sum_{c \in \mathcal{S}_i} w_{i,c}^{(t)} (1 - \max_{c' \in \mathcal{S}_i} \hat{p}_{i,c'}^{(t)} + \Phi(\hat{\mathbf{p}}_i^{(t)}))^\gamma \log(\hat{p}_{i,c}^{(t)}), \quad (14)$$

where $\hat{p}_{i,c}^{(t)}$ and $w_{i,c}^{(t)}$ denote the predicted probability and weight for the c -th class at the t -th epoch, respectively. γ denotes the exponential factor. The term $\max_{c' \in \mathcal{S}_i} \hat{p}_{i,c'}^{(t)}$ represents the maximum predicted probability among candidate labels, and $\Phi(\hat{\mathbf{p}}_i^{(t)})$ is a regularization term that enforces additional constraints on the probability distribution.

For non-candidate labels $\bar{c} \in \bar{\mathcal{S}}_i$, the weight $w_{i,\bar{c}}^{(t)}$ is maintained at zero for all epochs $t \in \{1, 2, \dots, T\}$, where T denotes the total number of training epochs. Conversely, for candidate labels $c \in \mathcal{S}_i$, the weight is initialized at $t = 1$

as $w_{i,c}^{(1)} = \frac{1}{|\mathcal{S}_i|}$ with $|\cdot|$ representing the set cardinality. For epochs $t \in \{2, 3, \dots, T\}$, the weight is updated as follows:

$$w_{i,c}^{(t)} = \alpha^{(t)} w_{i,c}^{(t-1)} + (1 - \alpha^{(t)}) \frac{\hat{p}_{i,c}^{(t)}}{\sum_{c \in \mathcal{S}_i} \hat{p}_{i,c}^{(t)}}, \quad (15)$$

where the parameter $\alpha^{(t)} = \frac{T-t}{T}$ regulates the update rate.

CDL can be instantiated in various ways by adjusting the transformation function $\Phi(\hat{\mathbf{p}}_i^{(t)})$. Specifically, we explore two distinct implementations: one where $\Phi(\hat{\mathbf{p}}_i^{(t)})$ is the second highest predicted probability among the candidate labels, i.e., $\Phi(\hat{\mathbf{p}}_i^{(t)}) = \max_{c' \in \mathcal{S}_i, c' \neq c} \hat{p}_{i,c'}^{(t)}$, and the corresponding loss function is defined as:

$$\mathcal{L}_{CDL-CC} = - \sum_{c \in \mathcal{S}_i} p_{i,c}^{(t)} (1 - \max_{c' \in \mathcal{S}_i} \hat{p}_{i,c'}^{(t)} + \max_{c' \in \mathcal{S}_i, c' \neq c} \hat{p}_{i,c'}^{(t)})^\gamma \log(\hat{p}_{i,c}^{(t)}), \quad (16)$$

and another in which $\Phi(\hat{\mathbf{p}}_i^{(t)})$ is the maximum predicted probability among non-candidate labels, i.e., $\Phi(\hat{\mathbf{p}}_i^{(t)}) = \max_{\bar{c} \in \bar{\mathcal{S}}_i} \hat{p}_{i,\bar{c}}^{(t)}$ is formulated as follows:

$$\mathcal{L}_{CDL-CN} = - \sum_{c \in \mathcal{S}_i} p_{i,c}^{(t)} (1 - \max_{c' \in \mathcal{S}_i} \hat{p}_{i,c'}^{(t)} + \max_{\bar{c} \in \bar{\mathcal{S}}_i} \hat{p}_{i,\bar{c}}^{(t)})^\gamma \log(\hat{p}_{i,c}^{(t)}). \quad (17)$$

The two CDL instantiations maintain the capacity of FL to address over-confidence while incorporating $\Phi(\hat{\mathbf{p}}_i^{(t)})$ to mitigate under-confidence, which provides a more balanced resolution of under-confidence and over-confidence compared to using FL or IFL alone. Moreover, CDL is designed to be plug-and-play, allowing for seamless integration with existing MIPL approaches. We propose a systematic integration of the two CDL instantiations with three established attention mechanisms: Disambiguation Attention Mechanism (DAM) [18], Scaled additive Attention Mechanism (SAM) [22], and Margin-aware Attention Mechanism (MAM) [23]. This integration yields six variants, i.e., DAMCC, DAMCN, SAMCC, SAMCN, MAMCC, and MAMCN.

4.3 Pseudo-Code of Calibratable Disambiguation Loss

Based on the provided dataset and parameters, Algorithm 1 presents the pseudo-code of our CDL. Initially, the algorithm uniformly initializes the weights of the candidate label set (Step 1). During each epoch, the training data is partitioned into multiple mini-batches (Step 3). The models then extract instance-level features and compute attention scores (Steps 5-6). These features are aggregated into bag-level representations for each mini-batch (Step 7). Subsequently, the model classifies each multi-instance bag and updates the weights of the candidate label set (Steps 8-9). Finally, the calibratable disambiguation loss is computed, and the model parameters are updated (Steps 10-11).

For unseen multi-instance bags, the process starts with extracting instance-level features using $\Psi(\cdot)$ (Step 14). Next, these features are aggregated into a bag-level representation using the attention mechanism DAM, SAM, or MAM (Step 15). Finally, the predicted label is obtained by selecting the category with the highest prediction probability (Step 16).

Algorithm 1 Pseudo-Code of CDL**Inputs:**

\mathcal{D} : MIPL training set $\{(\mathbf{X}_i, \mathcal{S}_i) \mid 1 \leq i \leq m\}$, where $\mathbf{X}_i = \{\mathbf{x}_{i,1}, \mathbf{x}_{i,2}, \dots, \mathbf{x}_{i,n_i}\}$, $\mathbf{x}_{i,j} \in \mathcal{X}$, $\mathcal{X} = \mathbb{R}^d$, $\mathcal{S}_i \subset \mathcal{Y}$, and $\mathcal{Y} = \{1, 2, \dots, k\}$

T : Total number of training epochs

\mathbf{X}_* : Unseen multi-instance bag with n_* instances

Outputs:

Y_* : Predicted label for $\mathbf{X}_* = \{\mathbf{x}_{i,1}, \mathbf{x}_{i,2}, \dots, \mathbf{x}_{i,n_*}\}$

Process:

- 1: Initialize the weights $w_{i,c}^{(1)} = \frac{1}{|\mathcal{S}_i|}$ for the candidate labels
- 2: **for** $t = 1$ to T **do**
- 3: Shuffle the training set \mathcal{D} into B mini-batches
- 4: **for** $b = 1$ to B **do**
- 5: Learn instance-level features using $\Psi(\cdot)$
- 6: Compute attention scores based on Eq. (8) for DAM, Eq. (9) for SAM, or Eqs. (10, 11, 12) for MAM
- 7: Aggregate instance-level features into bag-level features according to Eq. (13)
- 8: Classify the multi-instance bag and obtain predicted probabilities
- 9: Update the weights $w_{i,c}^{(t)}$ using Eq. (15)
- 10: Compute the calibratable disambiguation loss according to Eq. (16) or Eq. (17)
- 11: Update model parameters with the SGD optimizer
- 12: **end for**
- 13: **end for**
- 14: Learn instance-level features of the unknown multi-instance bag \mathbf{X}_* in the test set
- 15: Compute attention scores and aggregate instance-level features into a single vector \mathbf{z}_*
- 16: Return $Y_* = \arg \max_{c \in \mathcal{Y}} \hat{p}_{*,c}$

lower bound to MDL, providing theoretical guarantees for the optimization process. Second, it explicitly characterizes the regularization effect of CDL through the scaling factor $(1 - \gamma\beta_i)$. This regularization mechanism has two key implications: First, for multi-instance bags with low-confidence predictions (small values of β_i), the scaling factor $(1 - \gamma\beta_i)$ approaches 1, causing CDL to behave similarly to MDL. Second, for multi-instance bags with high-confidence predictions (large values of β_i), the scaling factor $(1 - \gamma\beta_i)$ decreases, effectively reducing the contribution of these samples to the overall loss.

To satisfy the theorem, the function $\Phi(\hat{\mathbf{p}}_i^{(t)})$ must lie within $[\max_{c' \in \mathcal{S}_i} \hat{p}_{i,c'}^{(t)} - 1, \max_{c' \in \mathcal{S}_i} \hat{p}_{i,c'}^{(t)}]$ at each iteration t . In practice, we explore two choices for $\Phi(\hat{\mathbf{p}}_i^{(t)})$:

- 1) $\Phi(\hat{\mathbf{p}}_i^{(t)}) = \max_{c' \in \mathcal{S}_i, c' \neq c} \hat{p}_{i,c'}^{(t)}$, which satisfies the condition since $\max_{c' \in \mathcal{S}_i, c' \neq c} \hat{p}_{i,c'}^{(t)} \leq \max_{c' \in \mathcal{S}_i} \hat{p}_{i,c'}^{(t)}$.
- 2) $\Phi(\hat{\mathbf{p}}_i^{(t)}) = \max_{\bar{c} \in \bar{\mathcal{S}}_i} \hat{p}_{i,\bar{c}}^{(t)}$, where $\bar{\mathcal{S}}_i$ represents the non-candidate label set. This choice holds as Fig. 7 demonstrates that predicted probabilities for candidate labels (true labels and false positive labels) significantly exceed those for non-candidate labels, ensuring $\max_{\bar{c} \in \bar{\mathcal{S}}_i} \hat{p}_{i,\bar{c}}^{(t)} \leq \max_{c' \in \mathcal{S}_i} \hat{p}_{i,c'}^{(t)}$. The weight update rule, as shown in Eq. (15), further reinforces this by assigning higher weights to candidate labels.

Consequently, CDL adaptively down-weights samples that the model finds easy to classify, i.e., those with high-confidence predictions, which prevents overfitting and improves generalization. The parameter γ serves as a control mechanism for this regularization effect, with larger values (within the valid range) amplifying the regularization. The complete proof of Theorem 1 is detailed in Appendix.

5 THEORETICAL EVIDENCE

In this section, we establish the theoretical foundation of the proposed Calibratable Disambiguation Loss (CDL) by analyzing its relationship with the Momentum-based Disambiguation Loss (MDL), which is pivotal in DEMIPL [18], ELIMIPL [22], and MIPLMA [23]. Our analysis demonstrates that CDL acts as an adaptive regularizer, bolstering the training process by dynamically modulating the contribution of each multi-instance bag.

Theorem 1 (Lower Bound and Regularization Properties of CDL). *Let \mathcal{L}_{CDL} denote the Calibratable Disambiguation Loss and \mathcal{L}_{MDL} denote the Momentum-based Disambiguation Loss. For any multi-instance bag \mathbf{X}_i with the candidate label set \mathcal{S}_i , under the condition that $\Phi(\hat{\mathbf{p}}_i^{(t)}) \in [\max_{c' \in \mathcal{S}_i} \hat{p}_{i,c'}^{(t)} - 1, \max_{c' \in \mathcal{S}_i} \hat{p}_{i,c'}^{(t)}]$, the following inequality holds:*

$$\mathcal{L}_{CDL} \geq (1 - \gamma\beta_i)\mathcal{L}_{MDL} = (1 - \gamma\beta_i)(\text{KL}(w_i \parallel \hat{\mathbf{p}}_i) + \mathbb{H}[w_i]), \quad (18)$$

where $\beta_i = \max_{c' \in \mathcal{S}_i} \hat{p}_{i,c'}^{(t)} - \Phi(\hat{\mathbf{p}}_i^{(t)})$ represents the confidence margin of the multi-instance bag \mathbf{X}_i , $\gamma \in [1, \frac{1}{\beta_{\max}}]$ controls the regularization strength, and $\beta_{\max} = \max_i \beta_i$ is the maximum confidence margin across all multi-instance bags in the dataset.

The theorem above reveals several important properties of our proposed CDL. First, it establishes a formal

6 EXPERIMENTS

6.1 Experimental Configurations

6.1.1 Datasets

We adopt the experimental protocol established by the prior research [18], which includes a diverse range of datasets, including four benchmark datasets and seven real-world datasets. Specifically, the benchmark datasets are MNIST-MIPL, FMNIST-MIPL, Birdsong-MIPL, and SIVAL-MIPL, which span various domains from image analysis to biological data [37], [58], [59], [60]. Additionally, we include CRC-MIPL, a real-world dataset for colorectal cancer classification. The candidate label sets are curated by professionally trained crowdsourcing workers. In the prior research [18], [22], four types of multi-instance features have been employed across different sub-datasets: CRC-MIPL-Row (C-Row), CRC-MIPL-SBN (C-SBN), CRC-MIPL-KMeansSeg (C-KMeans), and CRC-MIPL-SIFT (C-SIFT). These features are generated by four image bag generators, including Row, single blob with neighbors (SBN), k-means segmentation (KMeansSeg), and scale-invariant feature transformation function (SIFT).

Furthermore, a novel feature extraction strategy is proposed for the CRC-MIPL dataset by leveraging ResNet-34. Each image is partitioned into N non-overlapping patches, and ResNet-34 is applied to obtain feature representations for each patch. Three configurations are investigated, with

TABLE 1

Characteristics of the benchmark and real-world MIPL datasets. The C-R34-9 dataset is introduced in this work as a new MIPL dataset. "n/a" is abbreviated for not applicable as the instance-level labels of the CRC-MIPL dataset are unknown.

Dataset	#bag	#ins	max. #ins	min. #ins	avg. #ins	max. #pos	min. #pos	avg. #pos	#dim	#C	avg. #CLs
MNIST-MIPL	500	20664	48	35	41.33	9.1%	7.0%	8.0%	784	5	2, 3, 4
FMNIST-MIPL	500	20810	48	36	41.62	9.1%	7.0%	8.0%	784	5	2, 3, 4
Birdsong-MIPL	1300	48425	76	25	37.25	10.0%	6.9%	8.3%	38	13	2, 3, 4
SIVAL-MIPL	1500	47414	32	31	31.61	90.62%	3.12%	25.6%	30	25	2, 3, 4
C-Row	7000	56000	8	8	8	n/a	n/a	n/a	9	7	2.08
C-SBN	7000	63000	9	9	9	n/a	n/a	n/a	15	7	2.08
C-KMeans	7000	30178	6	3	4.311	n/a	n/a	n/a	6	7	2.08
C-SIFT	7000	175000	25	25	25	n/a	n/a	n/a	128	7	2.08
C-R34-9	7000	63000	9	9	9	n/a	n/a	n/a	1000	7	2.08
C-R34-16	7000	112000	16	16	16	n/a	n/a	n/a	1000	7	2.08
C-R34-25	7000	175000	25	25	25	n/a	n/a	n/a	1000	7	2.08

N set to 9, 16, and 25, resulting in the new datasets C-R34-9, C-R34-16, and C-R34-25, respectively. Notably, the C-R34-9 dataset is first introduced in this work. Table 1 provides further details on these datasets. More information on the benchmark datasets and the CRC-MIPL dataset can be found in literature [19] and [18], respectively.

6.1.2 Comparative Methods

To our knowledge, there are six available methods relevant to our MIPL settings, namely MIPLGP [19], DEMIPL [18], ELIMIPL [22], MIPLMA [23], PROMIPL [43], and FASTMIPL [44]. All corresponding code implementations for these methods are publicly available. We systematically compare our six methods against the six MIPL methods to evaluate their classification accuracy and calibration performance. The parameters for all compared methods were set following the recommendations from the original literature or were further optimized to enhance performance.

6.1.3 Implementation Details

Our algorithm is implemented using PyTorch and executed on an NVIDIA Tesla V100 GPU¹. We utilize stochastic gradient descent (SGD) with a momentum of 0.9 and a weight decay of 0.0001 for optimization. We adopt the same feature extractor $\Psi(\cdot)$ as used in previous MIPL methods [18], [22], [23], [43], [44]. For MNIST-MIPL and FMNIST-MIPL, we extract instance-level features using a two-layer convolutional neural network followed by a fully connected network. For preprocessed datasets, i.e., Birdsong-MIPL and SIVAL-MIPL, we use a fully connected network for feature extraction. For CRC-MIPL, we explore four image bag generators and use ResNet-34 to extract instance-level features. We select the learning rate from $\{0.01, 0.05\}$ and adjust it using cosine annealing. DAMCC and DAMCN are trained for 200 epochs on CRC-MIPL and 100 epochs on benchmark datasets. Meanwhile, SAMCC, SAMCN, MAMCC, and MAMCN are trained for 100 epochs on all datasets. We set the CDL parameter γ to 1 in all experiments. We report the mean and standard deviation (std) of classification accuracy and expected calibration error over ten random train/test splits with a ratio of 7:3. In our experiments, the expected calibration error is evaluated with 15 bins.

1. The code will be publicly available.

6.2 Classification Performance

6.2.1 Accuracy on the Benchmark Datasets

Table 2 demonstrates that our methods outperform the comparative methods in 67 of the 72 cases. In 12 of the 72 cases, the improvement exceeds 10%. FASTMIPL outperforms our models in 4 of the 72 cases. We speculate that FASTMIPL benefits from training all samples in a single batch, leveraging greater computational resources.

For MNIST-MIPL, the potential for accuracy improvement is limited for $r = 1$ and 2. However, for $r = 3$, DAMCC and SAMCC achieve significant accuracy improvements of 14.37% and 13.60%, respectively. Notably, MAMCC and MAMCN surpass MIPLMA by 20.14% and 23.07% on MNIST-MIPL with $r = 3$. On the FMNIST-MIPL and Birdsong-MIPL datasets, DAMCN achieves improvements exceeding 18%. Furthermore, on SIVAL-MIPL, both DAMCC and DAMCN achieve gains exceeding 10% for $r \in \{1, 2, 3\}$, with a peak improvement of 18.58%. As r increases from 1 to 3, the mean accuracy improvement across benchmark datasets is 3.27%, 4.57%, and 8.93%. These results indicate that CDL effectively handles more challenging scenarios.

6.2.2 Accuracy on the Real-World Datasets

The experimental results in Table 3 demonstrate that our methods consistently achieve superior classification accuracy compared to all baseline methods. Some MIPLGP results are marked as "--" due to computational limitations, which hinder evaluation on certain datasets. This limitation indicates that MIPLGP may struggle to integrate with deep learning-based feature representations.

The integration of CDL with DAM, SAM, or MAM consistently improves classification performance over DEMIPL, ELIMIPL, and MIPLMA. On the C-KMeans dataset, DAMCC and DAMCN achieve significant accuracy improvements of 10.67% and 12.67%, respectively. For image bag generators such as Row, SBN, and KMeans, DAM outperforms SAM and MAM in classification accuracy. In contrast, for instance-level feature learning with SIFT or ResNet-34, SAM and MAM outperform DAM. Furthermore, in the three CRC-MIPL datasets utilizing ResNet-34, all MIPL approaches exhibit improved performance as the number of partitioned patches increases. This trend indicates that in CRC-MIPL datasets, leveraging deep learning-based features contributes to enhancing classification performance.

TABLE 2

Classification accuracy (mean±std%) on the benchmark datasets with varying numbers of false positive labels ($r \in \{1, 2, 3\}$). The highest accuracy for each dataset is in boldface. \uparrow indicates improvements relative to DEMIPL [18], ELIMIPL [22], or MIPLMA [23].

	MNIST-MIPL	FMNIST-MIPL	Birdsong-MIPL	SIVAL-MIPL
$r = 1$				
MIPLGP	94.87±1.55	84.67±2.98	71.62±2.59	66.87±1.95
PROMIPL	99.92±0.29	92.20±2.39	77.63±1.50	68.20±3.22
FASTMIPL	99.91±0.23	90.99±2.19	79.60±2.35	77.65±3.02
DEMIPL	97.60±0.80	88.01±2.08	74.36±1.57	63.53±4.10
DAMCC (ours)	99.33±0.52 (1.73 \uparrow)	92.07±2.18 (4.06 \uparrow)	79.03±1.49 (4.67 \uparrow)	73.87±2.25 (10.34 \uparrow)
DAMCN (ours)	99.40±0.55 (5.13 \uparrow)	91.87±1.90 (3.86 \uparrow)	80.38±2.11 (6.02 \uparrow)	75.49±1.99 (11.96 \uparrow)
ELIMIPL	99.20±0.65	90.27±1.84	77.13±1.80	67.49±2.18
SAMCC (ours)	99.80±0.43 (0.60 \uparrow)	90.27±1.98 (0.00 \uparrow)	79.21±2.26 (2.08 \uparrow)	71.96±2.34 (4.47 \uparrow)
SAMCN (ours)	99.73±0.44 (0.53 \uparrow)	90.33±2.09 (0.06 \uparrow)	79.54±1.97 (2.41 \uparrow)	73.64±1.75 (6.15 \uparrow)
MIPLMA	98.47±1.03	91.53±1.61	77.56±2.05	70.33±2.63
MAMCC (ours)	99.93±0.20 (1.46 \uparrow)	92.73±1.21 (1.20 \uparrow)	79.54±1.59 (1.98 \uparrow)	72.40±1.86 (2.07 \uparrow)
MAMCN (ours)	99.93±0.20 (1.46 \uparrow)	93.20±1.33 (1.67 \uparrow)	79.95±1.23 (0.41 \uparrow)	74.40±2.21 (4.07 \uparrow)
$r = 2$				
MIPLGP	81.73±3.01	79.07±2.74	67.18±1.50	61.31±2.61
PROMIPL	99.86±0.24	88.83±2.26	71.84±1.96	63.35±2.32
FASTMIPL	99.77±0.41	90.15±2.53	78.91±2.29	70.72±2.67
DEMIPL	94.27±2.72	82.33±2.85	70.13±2.40	55.40±5.09
DAMCC (ours)	99.40±0.81 (5.13 \uparrow)	89.33±2.88 (7.00 \uparrow)	77.03±1.64 (6.90 \uparrow)	70.24±2.39 (14.84 \uparrow)
DAMCN (ours)	99.53±0.60 (5.26 \uparrow)	89.40±2.69 (7.07 \uparrow)	78.00±1.54 (7.87 \uparrow)	71.93±1.82 (16.53 \uparrow)
ELIMIPL	98.67±0.99	84.53±2.56	74.46±1.53	61.58±2.54
SAMCC (ours)	98.80±0.83 (0.13 \uparrow)	85.33±3.24 (0.80 \uparrow)	77.21±2.03 (2.75 \uparrow)	66.02±2.79 (4.44 \uparrow)
SAMCN (ours)	98.93±0.85 (0.26 \uparrow)	85.40±2.88 (0.87 \uparrow)	77.54±2.20 (3.08 \uparrow)	66.87±2.32 (5.29 \uparrow)
MIPLMA	97.87±1.39	86.67±2.76	76.15±1.55	66.82±3.10
MAMCC (ours)	99.80±0.31 (1.93 \uparrow)	89.47±1.86 (2.80 \uparrow)	77.36±2.13 (1.21 \uparrow)	69.91±2.34 (3.09 \uparrow)
MAMCN (ours)	99.87±0.27 (2.00 \uparrow)	90.07±1.50 (3.40 \uparrow)	78.46±1.92 (2.31 \uparrow)	71.42±1.75 (4.60 \uparrow)
$r = 3$				
MIPLGP	62.13±6.39	67.00±5.24	62.51±1.47	56.93±3.21
PROMIPL	78.32±11.64	65.89±4.14	69.33±2.11	53.88±2.41
FASTMIPL	97.43±7.37	81.60±7.01	77.30±2.24	61.49±3.48
DEMIPL	70.93±8.83	65.73±2.48	69.62±2.39	50.31±1.84
DAMCC (ours)	85.27±9.06 (14.37 \uparrow)	72.87±7.20 (7.14 \uparrow)	76.90±1.73 (7.28 \uparrow)	66.76±2.40 (16.45 \uparrow)
DAMCN (ours)	78.73±15.67 (7.80 \uparrow)	74.60±4.63 (8.87 \uparrow)	77.69±1.75 (8.07 \uparrow)	68.89±1.94 (18.58 \uparrow)
ELIMIPL	74.80±14.41	70.20±5.54	71.67±1.67	60.02±2.89
SAMCC (ours)	88.40±9.09 (13.60 \uparrow)	72.53±7.86 (2.33 \uparrow)	75.13±2.17 (3.46 \uparrow)	61.62±1.93 (1.60 \uparrow)
SAMCN (ours)	86.13±9.48 (11.33 \uparrow)	74.27±4.09 (4.07 \uparrow)	77.05±1.46 (5.38 \uparrow)	63.16±1.94 (3.14 \uparrow)
MIPLMA	74.93±10.32	65.40±5.53	74.56±1.29	62.73±2.38
MAMCC (ours)	95.07±7.26 (20.14 \uparrow)	74.00±7.57 (8.60 \uparrow)	77.18±1.57 (2.62 \uparrow)	67.20±2.73 (4.47 \uparrow)
MAMCN (ours)	98.00±1.49 (23.07 \uparrow)	77.73±4.95 (12.33 \uparrow)	77.82±1.32 (3.26 \uparrow)	69.13±1.47 (6.40 \uparrow)

TABLE 3

Classification accuracy (mean±std%) on the real-world datasets. The highest accuracy for each dataset is in boldface. \uparrow indicates improvements relative to DEMIPL [18], ELIMIPL [22], or MIPLMA [23]. – indicates computational constraints.

	C-Row	C-SBN	C-KMeans	C-SIFT	C-R34-9	C-R34-16	C-R34-25
MIPLGP	43.13±0.57	33.49±0.63	32.90±1.25	–	–	–	–
PROMIPL	43.51±0.93	51.56±1.23	56.52±1.30	56.25±1.11	60.62±1.02	64.63±0.75	67.24±0.80
FASTMIPL	48.68±3.81	57.21±3.08	57.30±1.28	52.55±2.95	56.78±1.61	61.85±1.48	64.24±1.64
DEMIPL	40.78±1.01	48.58±1.40	52.11±1.20	53.17±1.27	58.84±1.40	62.34±0.82	65.19±0.85
DAMCC (ours)	48.10±0.60 (7.32 \uparrow)	56.54±0.84 (7.96 \uparrow)	62.78±1.30 (10.67 \uparrow)	53.59±1.05 (0.42 \uparrow)	62.13±1.21 (3.29 \uparrow)	63.99±0.87 (1.65 \uparrow)	65.34±0.74 (0.15 \uparrow)
DAMCN (ours)	49.06±0.71 (8.28 \uparrow)	57.91±0.60 (9.33 \uparrow)	64.78±1.02 (12.67 \uparrow)	55.34±1.05 (2.17 \uparrow)	63.74±0.94 (4.90 \uparrow)	64.97±1.00 (2.63 \uparrow)	66.64±0.85 (1.45 \uparrow)
ELIMIPL	43.26±0.82	50.90±0.79	54.58±1.18	54.05±1.02	60.97±1.22	63.08±0.66	66.50±0.67
SAMCC (ours)	46.58±0.57 (3.32 \uparrow)	55.91±0.95 (5.01 \uparrow)	62.04±1.78 (7.46 \uparrow)	57.20±0.94 (3.15 \uparrow)	63.95±0.98 (2.98 \uparrow)	67.41±0.70 (4.33 \uparrow)	69.43±0.94 (2.93 \uparrow)
SAMCN (ours)	47.50±0.54 (4.24 \uparrow)	57.24±0.90 (6.34 \uparrow)	63.84±1.01 (9.26 \uparrow)	57.10±0.76 (3.05 \uparrow)	64.58±1.07 (3.61 \uparrow)	67.81±0.72 (4.73 \uparrow)	69.75±0.83 (3.25 \uparrow)
MIPLMA	44.37±0.99	52.46±0.70	55.78±16.89	55.29±0.94	59.38±1.24	63.12±0.77	68.70±1.08
MAMCC (ours)	47.66±0.57 (3.29 \uparrow)	56.83±1.06 (4.37 \uparrow)	57.60±1.28 (1.82 \uparrow)	56.97±0.97 (1.68 \uparrow)	64.74±0.98 (5.36 \uparrow)	67.88±0.85 (4.76 \uparrow)	69.83±0.96 (1.13 \uparrow)
MAMCN (ours)	47.99±0.50 (4.24 \uparrow)	57.40±0.94 (4.94 \uparrow)	59.02±0.96 (3.24 \uparrow)	57.07±0.86 (5.35 \uparrow)	64.73±1.02 (5.35 \uparrow)	67.72±0.78 (4.60 \uparrow)	69.81±1.00 (1.11 \uparrow)

Additionally, DAM performs well on simple feature representations in the CRC-MIPL dataset but struggles with complex ones. In contrast, SAM and MAM excel at complex

feature representations in the CRC-MIPL dataset but are not the best with simpler ones. Therefore, the choice of attention mechanism should align with the dataset’s feature com-

TABLE 4

Expected calibration error (mean \pm std%) on the benchmark datasets with varying numbers of false positive labels ($r \in \{1, 2, 3\}$). The minimum error for each dataset is in boldface. \downarrow denotes reductions in error relative to DEMIPL [18], ELIMIPL [22], or MIPLMA [23].

	MNIST-MIPL	FMNIST-MIPL	Birdsong-MIPL	SIVAL-MIPL
$r = 1$				
PROMIPL	59.62 \pm 0.16	53.56 \pm 2.20	60.77 \pm 1.52	59.46 \pm 3.12
FASTMIPL	3.47 \pm 0.54	5.53 \pm 1.35	7.15 \pm 1.72	10.90\pm2.11
DEMIPL	59.40 \pm 0.77	51.50 \pm 1.54	57.86 \pm 1.16	56.89 \pm 3.01
DAMCC (ours)	1.08 \pm 0.41 (58.32 \downarrow)	5.09 \pm 1.05 (46.41 \downarrow)	4.68 \pm 1.10 (53.18 \downarrow)	12.74 \pm 1.63 (44.15 \downarrow)
DAMCN (ours)	1.11 \pm 0.38 (58.29 \downarrow)	5.44 \pm 1.49 (46.06 \downarrow)	7.53 \pm 1.63 (50.33 \downarrow)	16.25 \pm 1.71 (40.64 \downarrow)
ELIMIPL	59.26 \pm 0.38	51.55 \pm 1.44	60.16 \pm 1.83	58.83 \pm 2.15
SAMCC (ours)	1.45 \pm 0.38 (57.81 \downarrow)	5.60 \pm 1.64 (45.95 \downarrow)	5.85 \pm 1.43 (54.31 \downarrow)	12.85 \pm 1.52 (45.98 \downarrow)
SAMCN (ours)	1.34 \pm 0.35 (57.92 \downarrow)	5.75 \pm 1.04 (45.80 \downarrow)	6.32 \pm 2.26 (53.84 \downarrow)	16.75 \pm 1.49 (42.08 \downarrow)
MIPLMA	58.65 \pm 0.85	52.38 \pm 1.60	60.89 \pm 2.04	61.67 \pm 2.58
MAMCC (ours)	1.00 \pm 0.15 (57.65 \downarrow)	4.84 \pm 1.43 (47.54 \downarrow)	4.53\pm0.68 (56.36 \downarrow)	12.15 \pm 1.02 (49.52 \downarrow)
MAMCN (ours)	0.94\pm0.17 (57.71 \downarrow)	4.18\pm1.57 (48.20 \downarrow)	6.87 \pm 1.75 (54.02 \downarrow)	15.91 \pm 1.38 (45.76 \downarrow)
$r = 2$				
PROMIPL	59.64 \pm 0.20	50.57 \pm 1.96	55.76 \pm 1.76	54.83 \pm 2.21
FASTMIPL	11.05 \pm 1.31	10.02 \pm 1.98	5.34 \pm 1.19	11.395 \pm 2.07
DEMIPL	59.62 \pm 1.09	48.84 \pm 2.18	51.65 \pm 1.63	51.55 \pm 3.68
DAMCC (ours)	1.20 \pm 0.58 (58.42 \downarrow)	6.62 \pm 2.04 (42.22 \downarrow)	5.23 \pm 0.74 (46.42 \downarrow)	10.32\pm1.20 (41.23 \downarrow)
DAMCN (ours)	0.86\pm0.42 (58.76 \downarrow)	6.33 \pm 2.41 (42.51 \downarrow)	5.54 \pm 1.38 (46.11 \downarrow)	14.45 \pm 1.63 (37.10 \downarrow)
ELIMIPL	60.02 \pm 1.04	48.89 \pm 2.55	57.77 \pm 1.56	53.18 \pm 2.49
SAMCC (ours)	3.13 \pm 0.51 (56.89 \downarrow)	7.53 \pm 1.35 (41.36 \downarrow)	4.98\pm0.83 (52.79 \downarrow)	10.66 \pm 1.81 (42.52 \downarrow)
SAMCN (ours)	2.72 \pm 0.32 (57.30 \downarrow)	6.93 \pm 1.74 (41.96 \downarrow)	6.70 \pm 1.21 (51.07 \downarrow)	16.53 \pm 1.97 (36.65 \downarrow)
MIPLMA	59.31 \pm 1.11	48.54 \pm 3.00	59.50 \pm 1.61	58.31 \pm 3.07
MAMCC (ours)	1.20 \pm 0.26 (58.11 \downarrow)	6.26\pm1.30 (42.28 \downarrow)	5.01 \pm 0.73 (54.49 \downarrow)	10.60 \pm 1.54 (47.71 \downarrow)
MAMCN (ours)	1.16 \pm 0.26 (58.15 \downarrow)	6.46 \pm 1.71 (42.08 \downarrow)	5.71 \pm 0.97 (53.79 \downarrow)	14.38 \pm 1.59 (43.93 \downarrow)
$r = 3$				
PROMIPL	46.41 \pm 11.20	35.26 \pm 4.25	54.40 \pm 2.22	45.89 \pm 2.26
FASTMIPL	21.46 \pm 3.29	16.92\pm4.35	6.77 \pm 1.24	13.91 \pm 2.48
DEMIPL	44.55 \pm 12.76	40.04 \pm 3.27	53.42 \pm 1.19	46.26 \pm 2.70
DAMCC (ours)	12.99 \pm 7.43 (31.56 \downarrow)	23.28 \pm 6.11 (16.76 \downarrow)	5.63 \pm 0.88 (47.79 \downarrow)	9.48 \pm 1.60 (36.78 \downarrow)
DAMCN (ours)	17.99 \pm 13.08 (26.56 \downarrow)	22.16 \pm 4.02 (17.88 \downarrow)	4.52\pm0.87 (48.90 \downarrow)	15.09 \pm 2.06 (31.17 \downarrow)
ELIMIPL	43.59 \pm 15.00	40.65 \pm 5.38	55.31 \pm 1.64	51.63 \pm 2.85
SAMCC (ours)	9.92 \pm 7.18 (33.67 \downarrow)	22.70 \pm 7.34 (17.95 \downarrow)	5.03 \pm 0.89 (50.28 \downarrow)	9.05 \pm 1.45 (42.58 \downarrow)
SAMCN (ours)	11.24 \pm 7.52 (32.35 \downarrow)	20.89 \pm 4.20 (19.76 \downarrow)	4.87 \pm 1.04 (50.44 \downarrow)	15.35 \pm 2.51 (36.28 \downarrow)
MIPLMA	44.90 \pm 10.56	38.04 \pm 5.32	58.02 \pm 1.22	54.35 \pm 2.33
MAMCC (ours)	4.55 \pm 5.62 (40.35 \downarrow)	21.33 \pm 7.25 (16.71 \downarrow)	5.55 \pm 1.12 (52.47 \downarrow)	8.88\pm1.45 (45.47 \downarrow)
MAMCN (ours)	1.72\pm0.92 (43.18 \downarrow)	18.90 \pm 4.59 (19.14 \downarrow)	5.34 \pm 1.32 (52.68 \downarrow)	14.02 \pm 1.42 (40.33 \downarrow)

plexity. For simple feature representations, DAM is optimal, whereas complex representations, such as those derived from deep learning-based feature extractors, benefit from the advanced capabilities of SAM and MAM.

6.3 Calibration Performance

6.3.1 ECE on the Benchmark Datasets

Table 4 displays the expected calibration error for our methods with five comparative MIPL methods on the benchmark datasets. Notably, MIPLGP follows the instance-space paradigm, where bag-level predicted labels are aggregated from the instance-level predictions. This method fits the predicted probability and label to the most prominent instance rather than the entire multi-instance bag. Consequently, MIPLGP generally underperforms compared to MIPL approaches based on the embedded-space paradigm. Therefore, we exclude the calibration results for MIPLGP.

The calibration results demonstrate that our CDL significantly reduces the ECE on the MIPL datasets. On the benchmark datasets, CDL reduces the ECE by over 50% in 26 out of 60 cases, with the minimum reduction being 16.76%, the maximum reduction being 58.76%, and the mean reduction being 44.76%. Additionally, MAM outperforms DAM and SAM in most cases, which is consistent with the accuracy observed on the benchmark datasets.

To evaluate the calibration performance of our methods relative to baseline methods, we present reliability diagrams on the test set of the Birdsong-MIPL dataset. Fig. 5 presents the reliability diagrams on the Birdsong-MIPL dataset. The diagrams display the classification accuracies and ECE based on ten random runs. The baseline methods, DEMIPL, ELIMIPL, and MIPLMA, consistently produce predicted probabilities below 0.25. Although these methods achieve over 70% classification accuracy, their calibration performance is notably subpar. In contrast, our methods exhibit significant improvements in both calibration performance and classification performance.

6.3.2 ECE on the Real-World Datasets

Table 5 presents the expected calibration error across the real-world datasets, comparing our proposed methods against state-of-the-art methods in MIPL. Our proposed methods consistently achieve lower calibration error than all the comparative methods, demonstrating their effectiveness in improving model calibration. Notably, MAM yields the best overall performance, with MAMCC attaining the lowest ECE across most datasets. The most significant improvement occurs on C-R34-25, where MAMCC reduces the ECE by 33.32% compared to MIPLMA. Our methods achieve over a 10% reduction in ECE in 33 out of 42 cases. These

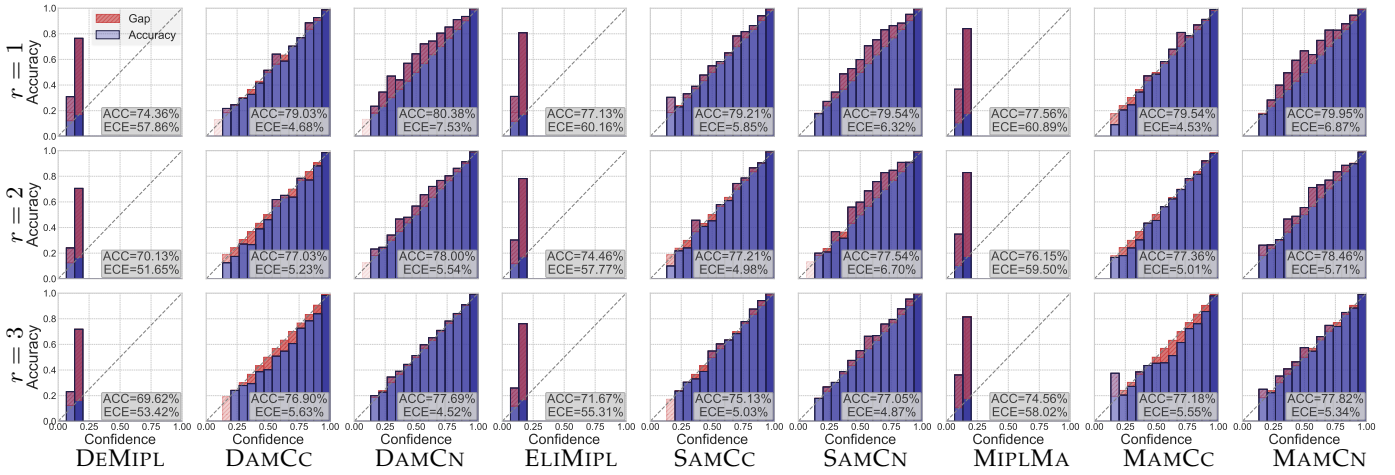


Fig. 5. Reliability diagrams of DEMIPL [18], ELIMIPL [22], and MIPLMA [23], and our methods on the Birdsong-MIPL datasets with varying numbers of false positive labels ($r \in \{1, 2, 3\}$). The bar color intensity indicates that more samples are assigned with the corresponding confidence intervals.

TABLE 5
Expected calibration error (mean \pm std%) on the real-world datasets. The minimum error for each dataset is in boldface. \downarrow denotes reductions in error relative to DEMIPL [18], ELIMIPL [22], or MIPLMA [23].

	C-Row	C-SBN	C-KMeans	C-SIFT	C-R34-9	C-R34-16	C-R34-25
PROMIPL	17.99 \pm 1.64	25.48 \pm 0.65	31.52 \pm 1.11	31.42 \pm 1.12	34.30 \pm 0.99	37.72 \pm 0.72	41.31 \pm 0.85
FASTMIPL	50.54 \pm 3.78	42.17 \pm 3.07	41.62 \pm 1.27	43.48 \pm 2.75	41.01 \pm 1.60	36.19 \pm 1.46	33.97 \pm 1.62
DEMIPL	16.40 \pm 1.06	22.59 \pm 1.10	27.82 \pm 1.09	28.17 \pm 0.99	32.89 \pm 1.37	36.37 \pm 0.80	39.23 \pm 0.85
DAMCC (ours)	16.10 \pm 0.57 (0.30 \downarrow)	15.13 \pm 0.61 (7.46 \downarrow)	10.39 \pm 0.71 (17.43 \downarrow)	23.42 \pm 1.21 (4.75 \downarrow)	20.90 \pm 1.37 (11.99 \downarrow)	20.42 \pm 0.84 (15.95 \downarrow)	19.83 \pm 0.98 (19.40 \downarrow)
DAMCN (ours)	10.54 \pm 0.86 (5.86 \downarrow)	12.12 \pm 0.57 (10.47 \downarrow)	9.67\pm0.44 (18.15 \downarrow)	21.38 \pm 1.08 (6.79 \downarrow)	19.96 \pm 0.78 (12.93 \downarrow)	20.12 \pm 0.77 (16.25 \downarrow)	19.59 \pm 1.01 (19.64 \downarrow)
ELIMIPL	18.21 \pm 0.83	24.91 \pm 0.78	28.99 \pm 1.18	28.76 \pm 1.04	34.47 \pm 1.17	36.70 \pm 0.67	40.24 \pm 0.66
SAMCC (ours)	15.52 \pm 0.51 (2.69 \downarrow)	14.58 \pm 0.93 (10.33 \downarrow)	10.83 \pm 0.69 (18.16 \downarrow)	17.73 \pm 0.86 (11.03 \downarrow)	18.38 \pm 1.03 (16.09 \downarrow)	16.88 \pm 0.60 (19.82 \downarrow)	16.04 \pm 0.87 (24.2 \downarrow)
SAMCN (ours)	9.82 \pm 0.86 (8.39 \downarrow)	10.66 \pm 0.60 (14.25 \downarrow)	10.95 \pm 1.27 (18.04 \downarrow)	18.91 \pm 0.68 (9.85 \downarrow)	20.45 \pm 0.93 (14.02 \downarrow)	18.53 \pm 0.71 (18.17 \downarrow)	16.11 \pm 0.84 (24.13 \downarrow)
MIPLMA	18.40 \pm 0.99	25.24 \pm 0.68	30.74 \pm 0.90	29.48 \pm 0.92	33.30 \pm 1.25	37.05 \pm 0.73	41.58 \pm 1.05
MAMCC (ours)	6.01\pm0.85 (12.39 \downarrow)	6.23\pm1.14 (19.01 \downarrow)	10.28 \pm 0.74 (20.46 \downarrow)	6.80 \pm 0.43 (22.68 \downarrow)	9.46\pm0.81 (23.84 \downarrow)	8.77\pm0.68 (28.28 \downarrow)	8.26\pm0.59 (33.32 \downarrow)
MAMCN (ours)	10.76 \pm 0.65 (8.39 \downarrow)	8.97 \pm 1.16 (16.27 \downarrow)	11.96 \pm 1.03 (18.78 \downarrow)	6.68\pm0.34 (22.8 \downarrow)	10.25 \pm 0.73 (23.05 \downarrow)	9.25 \pm 0.68 (27.8 \downarrow)	8.50 \pm 0.76 (33.08 \downarrow)

results indicate that our CDL effectively aligns predicted confidences with classification accuracies, thereby enhancing model calibration.

Our methods exhibit particularly strong performance gains on the C-R34-9, C-R34-16, and C-R34-25 datasets compared to previous MIPL methods such as DEMIPL, ELIMIPL, and MIPLMA. Specifically, when combined with DAM, SAM, or MAM, our CDL achieves up to 19%, 24%, and 33% lower ECE on the C-R34-25 dataset. These findings highlight our framework’s ability to leverage fine-grained image representations for improved calibration, demonstrating its effectiveness on challenging datasets.

6.4 Mechanisms Underlying the Effectiveness of CDL

The calibratable disambiguation loss (CDL) significantly improves both classification and calibration performances compared to baseline methods DEMIPL, ELIMIPL, and MIPLMA. To elucidate the reasons behind its effectiveness, we analyze its impact from two critical components of MIPL approaches based on the embedded-space paradigm: feature aggregation and label disambiguation.

6.4.1 Enhancing Feature Aggregation

To evaluate the impact on feature aggregation, we visualize the bag-level feature representations, i.e., z_i from Eq. (13), for both baseline methods DEMIPL, ELIMIPL, MIPLMA, and our proposed methods on the MNIST-MIPL dataset. Unlike the standard MNIST dataset, which comprises 10 target classes, the MNIST-MIPL dataset focuses on 5 target classes, with negative instances sourced from the remaining 5 classes [19]. For $r = 1$ and $r = 2$, DEMIPL, ELIMIPL, and MIPLMA produce reasonably good results. However, when $r = 3$, the feature representations aggregated by the three methods become increasingly disordered, with features from different classes becoming mixed. In contrast, our methods consistently produce well-separated feature representations for $r \in \{1, 2, 3\}$. Specifically, for $r = 1$ and $r = 2$, the class clusters are compact and distinctly separable. Although the clusters are somewhat dispersed at $r = 3$, our methods remain notably more distinct and separable compared to those generated by the baseline methods DEMIPL, ELIMIPL, and MIPLMA.

Therefore, the visualizations in Fig. 6 demonstrate that our proposed CDL significantly improves the aggregation

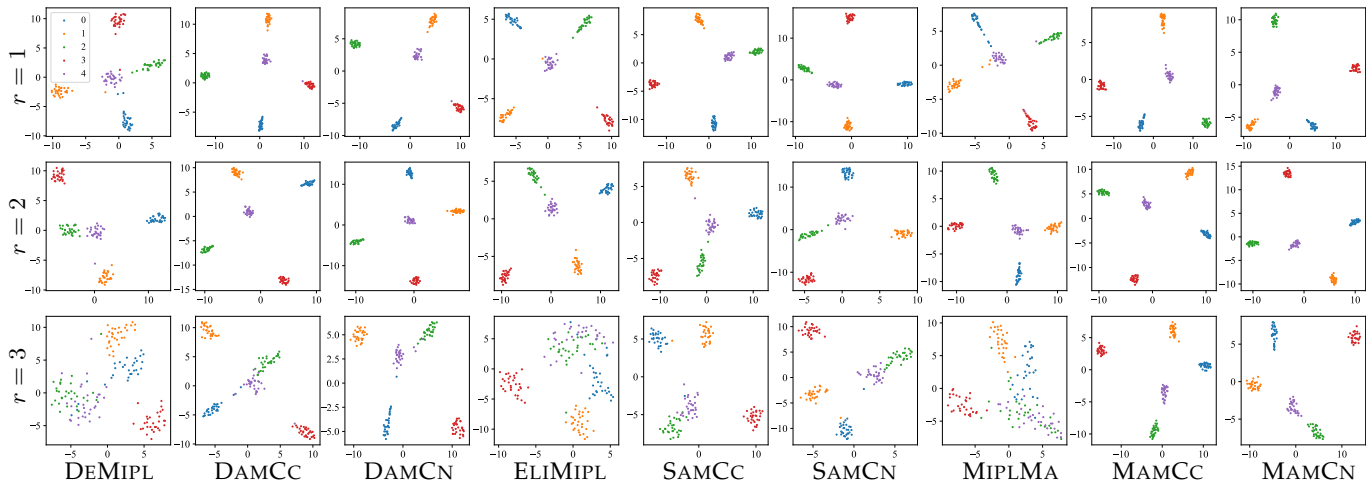


Fig. 6. t-SNE visualization of aggregated bag-level feature representations produced by the attention mechanisms in DEMIPL [18], ELIMIPL [22], MIPLMA [23], and ours on the test set of the MNIST-MIPL dataset, which comprises five classes.

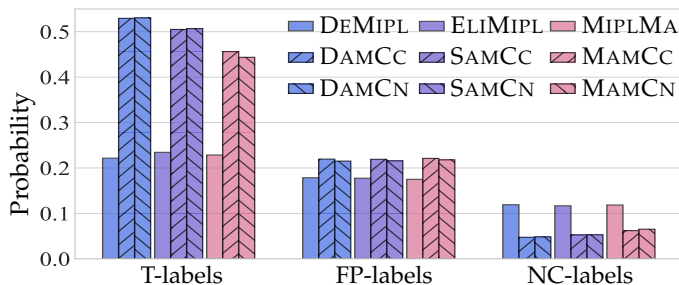


Fig. 7. Probabilities at the last epoch on the training set of the C-KMeans dataset. T-labels, FP-labels, and NC-labels denote the average probabilities for true, false positive, and non-candidate labels, respectively.

of bag-level feature representations, resulting in more compact and distinguishable clusters. This enhancement directly contributes to superior classification performance.

6.4.2 Optimizing Label Disambiguation and Calibration

The disambiguation performance and calibration performance of a model are directly influenced by its predicted probabilities. As shown in Fig. 2, the baseline methods DEMIPL, ELIMIPL, and MIPLMA generate low predicted probabilities for true labels on the training set, leading to poor calibration performance. In contrast, our methods yield significantly higher predicted probabilities for true labels compared to these baseline methods. To further investigate the effect of CDL on predicted probabilities, we present the average predicted probabilities for true labels (T-labels), false positive labels (FP-labels), and non-candidate labels (NC-labels) on the training set of the C-Kmeans dataset.

As illustrated in Fig. 7, for DEMIPL, ELIMIPL, and MIPLMA, the probabilities for true labels are comparable to those for false positive labels. In contrast, our methods achieve markedly higher probabilities for true labels compared to false positive labels. Although our methods also show higher probabilities for false positive labels relative to DEMIPL, ELIMIPL, and MIPLMA, the proportion of probabilities for false positive labels relative to candidate labels is substantially lower. Additionally, our methods achieve

significantly lower predicted probabilities for non-candidate labels compared to the baseline methods.

According to the definition of CDL, there exists an inverse relationship between the maximum predicted probabilities on candidate labels and the outcome of $\Phi(\cdot)$. For samples with high maximum predicted probabilities on candidate labels, the outcome of $\Phi(\cdot)$ is relatively small, resulting in lower loss values for these samples. Samples with low maximum predicted probabilities produce a larger outcome of $\Phi(\cdot)$, leading to higher loss values. Consequently, during training, the model emphasizes these high-loss samples, thereby enhancing their maximum predicted probabilities on candidate labels and further improving both calibration and disambiguation performance.

6.5 Further Analysis

6.5.1 Parameter Sensitivity

In our proposed CDL, the only hyperparameter is the exponential factor γ . Consistent with focal loss [48], [57], we treat γ as a constant throughout our experiments. To evaluate the sensitivity of our methods to γ , Fig. 8 presents the accuracy and expected calibration error of DEMIPL, ELIMIPL, MIPLMA, and our six methods with γ values ranging from $\{1, 2, 3, 4, 5\}$ on the C-R34-25 dataset.

Across all γ settings, our methods consistently outperform DEMIPL, ELIMIPL, and MIPLMA in both classification and calibration performance. As γ increases from 1 to 5, we observe a general improvement in calibration performance, though the gains diminish at higher values. Notably, ELIMIPL and MIPLMA exhibit greater robustness to variations in γ compared to DEMIPL, likely due to their relatively more sophisticated structure of the attention mechanisms, which provide better resistance to hyperparameter fluctuations. Furthermore, the two CDL instantiations yield comparable results, indicating that CDL’s effectiveness is largely independent of the specific instantiation.

6.5.2 Comparison with FL and IFL

To evaluate the effectiveness of CDL compared to focal loss (FL) and inverse focal loss (IFL), we integrate FL and IFL

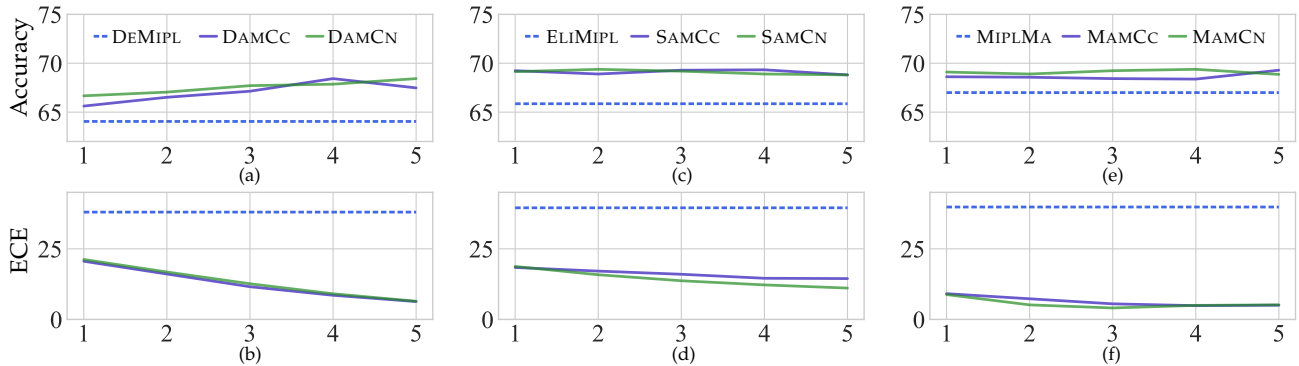


Fig. 8. Classification accuracy and expected calibration error of DEMIPL (a, b), ELIMIPL (c, d), MIPLMA (e, f), and our six methods on the C-R34-25 dataset for $\gamma \in \{1, 2, 3, 4, 5\}$. The horizontal axis represents γ .

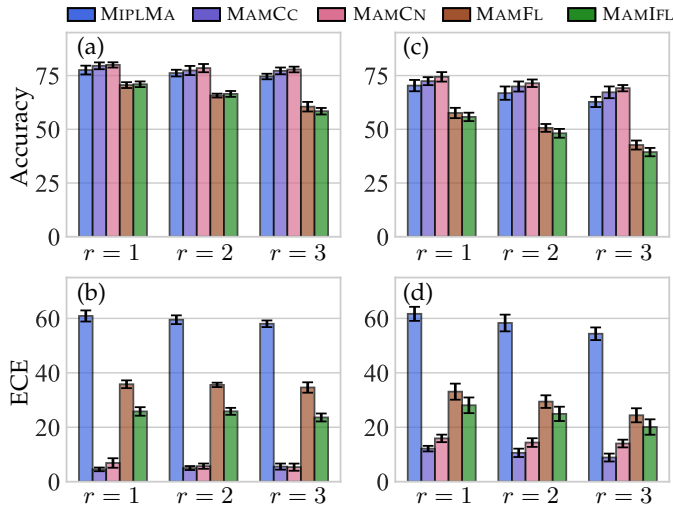


Fig. 9. Classification accuracy and expected calibration error (mean and std) of MAM, MAMCC, MAMCN, MAMFL, and MAMIFL on the Birdsong-MIPL (a, b) and SIVAL-MIPL (c, d) datasets.

into MAM, resulting in two variants: MAMFL and MAMIFL. The corresponding loss functions are defined in Eqs. (5) and (6), respectively, where the weights $w_{c,t}^{(t)}$ of candidate labels are initialized as $w_{i,c}^{(1)} = \frac{1}{|S_i|}$ at $t = 1$ and updated using Eq. (15). Therefore, the only distinction between MAMFL/MAMIFL and our proposed MAMCC/MAMCN lies in the exponential term of the loss functions.

Fig. 9 presents the classification accuracy and expected calibration error of MIPLMA, MAMCC, MAMCN, MAMFL, and MAMIFL on the Birdsong-MIPL and SIVAL-MIPL datasets, with the number of false positive labels $r \in \{1, 2, 3\}$. As shown in Fig. 9, MAMFL and MAMIFL improve the calibration of MIPLMA by reducing ECE. However, this improvement comes at the expense of classification accuracy, which declines more significantly as the number of false positive labels increases. Furthermore, both MAMFL and MAMIFL underperform compared to our proposed CDL in both classification and calibration. These findings indicate that FL and IFL are insufficient for handling classification and calibration challenges in MIPL.

6.5.3 Comparison with PLL Methods

We compare our methods with three popular PLL methods: PRODEN [24], LWS [41], and POP [15]. PRODEN is a classical

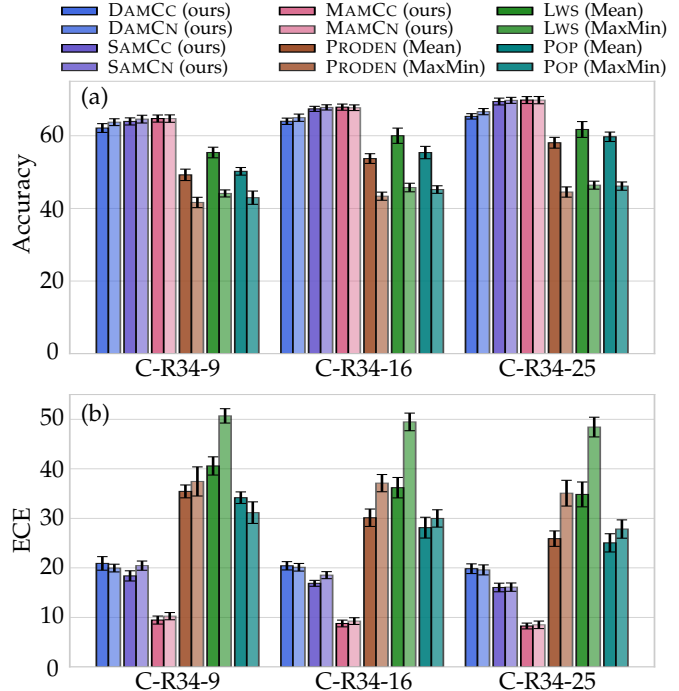


Fig. 10. Classification accuracy and expected calibration error (mean and std) of our six methods and three PLL methods on the CRC-MIPL datasets with ResNet-34 as the feature extractor.

PLL method based on deep learning that employs progressive disambiguation loss to identify true labels from candidate label sets. LWS introduces a weighted disambiguation loss to refine the true labels. POP is an instance-dependent PLL method that trains the classifier using progressive purification of candidate labels. To adapt MIPL data for PLL methods, we employ two strategies from the existing MIPL literature [19] to convert MIPL data into PLL data. 1) Mean: For each bag, we compute the average value of instances in each feature dimension as the representative feature value for that dimension. This strategy generates a holistic feature vector that retains the same dimensionality as the original instances. 2) MaxMin: We derive the maximum and minimum values across all instances for each feature dimension and concatenate these values. This strategy produces a holistic feature vector with a combined dimensionality of $2d$.

Fig. 10 presents the classification accuracy and expected

TABLE 6
Classification accuracy and expected calibration error (mean \pm std%) of POP, POP-CC, and POP-CN on the CRC-MIPL datasets using ResNet-34. The highest accuracy and the minimum error for each dataset is highlighted in bold.

	C-R34-9		C-R34-16		C-R34-25	
	Mean	MaxMin	Mean	MaxMin	Mean	MaxMin
	Accuracy					
POP	49.83 \pm 1.28	43.23 \pm 1.08	54.86 \pm 1.37	44.96 \pm 0.93	59.06 \pm 1.41	46.16 \pm 1.49
POP-CC	61.85 \pm 1.67	53.74\pm1.61	66.36 \pm 1.43	56.11\pm0.78	69.17 \pm 1.07	57.51 \pm 1.21
POP-CN	62.25\pm1.55	53.15 \pm 1.66	66.75\pm1.05	56.00 \pm 1.25	69.18\pm1.01	57.74\pm1.04
	ECE					
POP	25.01 \pm 1.43	29.74 \pm 2.01	22.00 \pm 1.22	28.87 \pm 1.23	19.49 \pm 1.52	27.26 \pm 1.41
POP-CC	16.91 \pm 2.14	18.50\pm2.21	13.90 \pm 1.38	16.98\pm1.54	12.94\pm1.27	16.29\pm1.53
POP-CN	16.66\pm1.45	19.53 \pm 1.83	13.70\pm1.31	17.13 \pm 1.71	13.08 \pm 1.05	16.35 \pm 1.60

calibration error of our six methods and the three PLL methods on the CRC-MIPL dataset using ResNet-34 features. Our methods consistently achieve the highest classification accuracy and the lowest expected calibration error across all three datasets. The results demonstrate that our methods substantially outperform the comparative PLL methods.

6.5.4 CDL for PLL Methods

The proposed CDL is a plug-and-play loss function that can be seamlessly incorporated into both MIPL and PLL frameworks. To adapt CDL for PLL, we propose two variants for POP [15], namely POP-CC and POP-CN. The POP-CC variant integrates the first instantiation \mathcal{L}_{CDL-CC} into POP, whereas POP-CN incorporates the second instantiation \mathcal{L}_{CDL-CN} .

Table 6 reports the classification accuracy and ECE of these three methods on the CRC-MIPL datasets, using features extracted by ResNet-34. Both variants significantly outperform the vanilla POP, achieving higher classification accuracy and lower expected calibration error, highlighting the effectiveness of CDL in improving both classification and calibration. Notably, the accuracy and expected calibration error of POP-CC and POP-CN are highly similar, indicating that both CDL instantiations are equally effective in enhancing POP’s classification and calibration capability.

6.6 Discussion

Our comprehensive evaluation confirms that CDL achieves state-of-the-art performance across the benchmark and real-world MIPL datasets. The experimental results highlight three key insights: (1) CDL significantly improves classification accuracy, particularly in high-ambiguity scenarios ($r = 3$), achieving a mean improvement of 8.93% on benchmark datasets. (2) CDL simultaneously enhances calibration, reducing ECE by an average of 44.76% on benchmark datasets due to its dynamic sample weighting mechanism. (3) Visualization analyses and probability distribution studies confirm that these improvements result from CDL’s ability to enforce distribution in feature spaces while adaptively prioritizing ambiguous labels during training.

The two instantiations of CDL consistently enhance both classification and calibration compared to the baseline models. In terms of classification accuracy, the second instantiation \mathcal{L}_{CDL-CN} outperforms \mathcal{L}_{CDL-CC} in most cases; conversely, \mathcal{L}_{CDL-CC} generally achieves lower expected calibration error than \mathcal{L}_{CDL-CN} . These observations lead to several insights: First, incorporating non-candidate label confidences can facilitate improved learning in MIPL models. Second, \mathcal{L}_{CDL-CC}

appears more effective when the candidate label set contains semantically similar labels. Third, \mathcal{L}_{CDL-CN} tends to perform better in scenarios with a high degree of label randomness, as commonly seen in benchmark datasets. Moreover, performance differences among the three attention mechanisms on real-world datasets suggest that architectural complexity should be matched to the characteristics of the feature space. For example, DAM is more efficient for relatively simple features, while SAM and MAM are better suited for complex representations. No single CDL instantiation or attention mechanism is optimal for both classification and calibration, highlighting the importance of selecting the appropriate combination based on specific task requirements.

7 CONCLUSION

This paper investigates the calibration performance of multi-instance partial-label learning. We propose a calibratable disambiguation loss (CDL) that improves both classification accuracy and expected calibration error. The proposed loss features two instantiations and can be seamlessly integrated with existing multi-instance partial-label learning (MIPL) and partial-label learning approaches. We provide theoretical insights validating CDL’s lower bound and regularization properties. Extensive experiments demonstrate CDL’s effectiveness, achieving superior classification performance in 105 out of 110 cases and superior calibration performance in 93 out of 95 cases compared to state-of-the-art MIPL approaches. These results highlight CDL’s robustness in handling high-ambiguity scenarios and improving the alignment between model confidence and accuracy.

While our approach demonstrates superior classification and calibration performance on challenging datasets like the C-R34-25 dataset, it does not achieve perfect calibration, where the expected calibration error reaches zero. To further improve calibration and classification under diverse conditions, we aim to develop more advanced calibration and disambiguation techniques, including adaptive loss formulations and uncertainty-aware learning frameworks.

REFERENCES

- [1] Z.-H. Zhou, “A brief introduction to weakly supervised learning,” *National Science Review*, vol. 5, no. 1, pp. 44–53, 2018.
- [2] J. Amores, “Multiple instance classification: Review, taxonomy and comparative study,” *Artificial Intelligence*, vol. 201, pp. 81–105, 2013.
- [3] M.-A. Carbonneau, V. Cheplygina, E. Granger, and G. Gagnon, “Multiple instance learning: A survey of problem characteristics and applications,” *Pattern Recognition*, vol. 77, pp. 329–353, 2018.

- [4] M. Ilse, J. M. Tomczak, and M. Welling, "Attention-based deep multiple instance learning," in *Proceedings of the 35th International Conference on Machine Learning, Stockholmsmässan, Stockholm, Sweden*, 2018, pp. 2132–2141.
- [5] X. Wang, Y. Yan, P. Tang, X. Bai, and W. Liu, "Revisiting multiple instance neural networks," *Pattern Recognition*, vol. 74, pp. 15–24, 2018.
- [6] W. Zhang, X. Zhang, H.-W. Deng, and M.-L. Zhang, "Multi-instance causal representation learning for instance label prediction and out-of-distribution generalization," in *Advances in Neural Information Processing Systems 35, New Orleans, LA, USA*, 2022, pp. 34 940–34 953.
- [7] H. Zhang, Y. Meng, Y. Zhao, Y. Qiao, X. Yang, S. E. Coupland, and Y. Zheng, "DTFD-MIL: Double-tier feature distillation multiple instance learning for histopathology whole slide image classification," in *Proceedings of the 35th IEEE/CVF Conference on Computer Vision and Pattern Recognition, New Orleans, USA*, 2022, pp. 18 802–18 812.
- [8] G. S. A. Hajj, A. Hubin, C. Kanduri, M. Pavlovic, K. D. Rand, M. Widrich, A. S. Solberg, V. Greiff, J. Pensar, G. Klambauer, and G. K. Sandve, "Incorporating probabilistic domain knowledge into deep multiple instance learning," in *Proceedings of the 41st International Conference on Machine Learning, Vienna, Austria*, 2024, pp. 17 279–17 297.
- [9] Y. Zhang, Z. Zhou, X. He, A. R. Adhikary, and B. Dutta, "Data-driven knowledge fusion for deep multi-instance learning," *IEEE Transactions on Neural Networks and Learning Systems*, pp. 1–15, 2024.
- [10] T. Cour, B. Sapp, and B. Taskar, "Learning from partial labels," *The Journal of Machine Learning Research*, vol. 12, pp. 1501–1536, 2011.
- [11] F. Zhang, L. Feng, B. Han, T. Liu, G. Niu, T. Qin, and M. Sugiyama, "Exploiting class activation value for partial-label learning," in *Proceedings of the 10th International Conference on Learning Representations, Virtual Event*, 2022, pp. 1–17.
- [12] S. He, L. Feng, F. Lv, W. Li, and G. Yang, "Partial label learning with semantic label representations," in *Proceedings of the 28th ACM SIGKDD Conference on Knowledge Discovery and Data Mining, Washington, DC, USA*, 2022, pp. 545–553.
- [13] X. Gong, D. Yuan, W. Bao, and F. Luo, "A unifying probabilistic framework for partially labeled data learning," *IEEE Transactions on Pattern Analysis and Machine Intelligence*, vol. 45, no. 7, pp. 8036–8048, 2023.
- [14] X. Li, Y. Jiang, C. Li, Y. Wang, and J. Ouyang, "Learning with partial labels from semi-supervised perspective," in *Proceedings of the 37th AAAI Conference on Artificial Intelligence, Washington, DC, USA*, 2023, pp. 8666–8674.
- [15] N. Xu, B. Liu, J. Lv, C. Qiao, and X. Geng, "Progressive purification for instance-dependent partial label learning," in *Proceedings of the 40th International Conference on Machine Learning, Honolulu, HI, USA*, ser. Proceedings of Machine Learning Research, vol. 202, 2023, pp. 38 551–38 565.
- [16] D.-D. Wu, D.-B. Wang, and M.-L. Zhang, "Distilling reliable knowledge for instance-dependent partial label learning," in *Proceedings of the 38th AAAI Conference on Artificial Intelligence, Vancouver, Canada*, 2024, pp. 15 888–15 896.
- [17] Y.-Z. Wang, W. Zhang, and M.-L. Zhang, "Partial label causal representation learning for instance-dependent supervision and domain generalization," in *Proceedings of the 39th AAAI Conference on Artificial Intelligence, Philadelphia, PA, USA*, Philadelphia, Pennsylvania, 2025, pp. 1–9.
- [18] W. Tang, W. Zhang, and M.-L. Zhang, "Disambiguated attention embedding for multi-instance partial-label learning," in *Advances in Neural Information Processing Systems 36, New Orleans, LA, USA*, 2023, pp. 56 756–56 771.
- [19] W. Tang, W. Zhang, and M.-L. Zhang, "Multi-instance partial-label learning: Towards exploiting dual inexact supervision," *Science China Information Sciences*, vol. 67, no. 3, pp. 132 103:1–132 103:14, 2024.
- [20] G. Campanella, M. G. Hanna, L. Geneslaw, A. Miraflor, V. Werneck Krauss Silva, K. J. Busam, E. Brogi, V. E. Reuter, D. S. Klimstra, and T. J. Fuchs, "Clinical-grade computational pathology using weakly supervised deep learning on whole slide images," *Nature Medicine*, vol. 25, no. 8, pp. 1301–1309, 2019.
- [21] A. Grote, N. S. Schaadt, G. Forestier, C. Wemmert, and F. Feuerhake, "Crowdsourcing of histological image labeling and object delineation by medical students," *IEEE Transactions Medical Imaging*, vol. 38, no. 5, pp. 1284–1294, 2019.
- [22] W. Tang, W. Zhang, and M.-L. Zhang, "Exploiting conjugate label information for multi-instance partial-label learning," in *Proceedings of the 33rd International Joint Conference on Artificial Intelligence, Jeju, South Korea*, 2024, pp. 4973–4981.
- [23] W. Tang, Y.-F. Yang, Z. Wang, W. Zhang, and M.-L. Zhang, "Multi-instance partial-label learning with margin adjustment," in *Advances in Neural Information Processing Systems 37, Vancouver, Canada*, 2024, pp. 26 331–26 354.
- [24] J. Lv, M. Xu, L. Feng, G. Niu, X. Geng, and M. Sugiyama, "Progressive identification of true labels for partial-label learning," in *Proceedings of the 37th International Conference on Machine Learning, Virtual Event*, 2020, pp. 6500–6510.
- [25] T. G. Dietterich, R. H. Lathrop, and T. Lozano-Pérez, "Solving the multiple instance problem with axis-parallel rectangles," *Artificial intelligence*, vol. 89, no. 1-2, pp. 31–71, 1997.
- [26] Z.-H. Zhou, Y.-Y. Sun, and Y.-F. Li, "Multi-instance learning by treating instances as non-i.i.d. samples," in *Proceedings of the 26th International Conference on Machine Learning, Montreal, Quebec, Canada*, 2009, pp. 1249–1256.
- [27] T. Yuan, F. Wan, M. Fu, J. Liu, S. Xu, X. Ji, and Q. Ye, "Multiple instance active learning for object detection," in *Proceedings of the 34th IEEE/CVF Conference on Computer Vision and Pattern Recognition, Virtual Event*, 2021, pp. 5330–5339.
- [28] H. Lv, Z. Yue, Q. Sun, B. Luo, Z. Cui, and H. Zhang, "Unbiased multiple instance learning for weakly supervised video anomaly detection," in *Proceedings of the 34th IEEE/CVF Conference on Computer Vision and Pattern Recognition, Vancouver, Canada*, 2023, pp. 8022–8031.
- [29] X. Shi, F. Xing, Y. Xie, Z. Zhang, L. Cui, and L. Yang, "Loss-based attention for deep multiple instance learning," in *Proceedings of the 34th AAAI Conference on Artificial Intelligence, New York, NY, USA*, 2020, pp. 5742–5749.
- [30] Y. Cui, Z. Liu, X. Liu, X. Liu, C. Wang, T.-W. Kuo, C. J. Xue, and A. B. Chan, "Bayes-MIL: A new probabilistic perspective on attention-based multiple instance learning for whole slide images," in *Proceedings of the 11th International Conference on Learning Representations, Kigali, Rwanda*, 2023, pp. 1–17.
- [31] O. Fourkioti, M. D. Vries, and C. Bakal, "CAMIL: context-aware multiple instance learning for cancer detection and subtyping in whole slide images," in *Proceedings of the 12th International Conference on Learning Representations, Vienna, Austria*, 2024, pp. 1–16.
- [32] J. Early, G. K. C. Cheung, K. Cutajar, H. Xie, J. Kandola, and N. Twomey, "Inherently interpretable time series classification via multiple instance learning," in *Proceedings of the 12th International Conference on Learning Representations, Vienna, Austria*, 2024, paper 1–29.
- [33] G. Lyu, S. Feng, T. Wang, C. Lang, and Y. Li, "GM-PLL: Graph matching based partial label learning," *IEEE Transactions on Knowledge and Data Engineering*, vol. 33, no. 2, pp. 521–535, 2019.
- [34] Y. Yao, J. Deng, X. Chen, C. Gong, J. Wu, and J. Yang, "Deep discriminative CNN with temporal ensembling for ambiguously-labeled image classification," in *Proceedings of the 34th AAAI Conference on Artificial Intelligence, New York, NY, USA*, 2020, pp. 12 669–12 676.
- [35] L. Liu and T. G. Dietterich, "A conditional multinomial mixture model for superset label learning," in *Advances in Neural Information Processing Systems 25, Cambridge, MA, USA*, 2012, pp. 548–556.
- [36] K. He, W. Tang, T. Wei, and M. Zhang, "Tuning the right foundation models is what you need for partial label learning," *CoRR*, vol. abs/2506.05027, 2025.
- [37] F. Briggs, X. Z. Fern, and R. Raich, "Rank-loss support instance machines for MIML instance annotation," in *Proceedings of the 18th ACM SIGKDD International Conference on Knowledge Discovery and Data Mining, Beijing, China*, 2012, pp. 534–542.
- [38] W. Wang and M. Zhang, "Semi-supervised partial label learning via confidence-rated margin maximization," in *Advances in Neural Information Processing Systems 33, Virtual Event*, 2020, pp. 6982–6993.
- [39] D.-B. Wang, M.-L. Zhang, and L. Li, "Adaptive graph guided disambiguation for partial label learning," *IEEE Transactions on Pattern Analysis and Machine Intelligence*, vol. 44, no. 12, pp. 8796–8811, 2022.
- [40] L. Feng, J. Lv, B. Han, M. Xu, G. Niu, X. Geng, B. An, and M. Sugiyama, "Provably consistent partial-label learning," in *Advances in Neural Information Processing Systems 33, Virtual Event*, 2020, pp. 10 948–10 960.

- [41] H. Wen, J. Cui, H. Hang, J. Liu, Y. Wang, and Z. Lin, "Leveraged weighted loss for partial label learning," in *Proceedings of the 38th International Conference on Machine Learning, Virtual Event*, 2021, pp. 11 091–11 100.
- [42] W. Wang, D.-D. Wu, J. Wang, G. Niu, M.-L. Zhang, and M. Sugiyama, "Realistic evaluation of deep partial-label learning algorithms," in *Proceedings of the 13th International Conference on Learning Representations, Singapore*, 2025, pp. 1–25.
- [43] Y.-F. Yang, W. Tang, and M.-L. Zhang, "ProMIP: A probabilistic generative model for multi-instance partial-label learning," in *Proceedings of the 24th IEEE International Conference on Data Mining, Abu Dhabi, UAE*, 2024, pp. 560–569.
- [44] Y.-F. Yang, W. Tang, and M.-L. Zhang, "Fast multi-instance partial-label learning," in *Proceedings of the 39th AAAI Conference on Artificial Intelligence, Philadelphia, PA, USA, Philadelphia, Pennsylvania*, 2025, pp. 1–9.
- [45] K. Wang, E. Tsamoura, and D. Roth, "On learning latent models with multi-instance weak supervision," in *Advances in Neural Information Processing Systems 36, New Orleans, LA, USA*, 2023, pp. 9661–9694.
- [46] C. Guo, G. Pleiss, Y. Sun, and K. Q. Weinberger, "On calibration of modern neural networks," in *Proceedings of the 34th International Conference on Machine Learning, Sydney, NSW, Australia*, 2017, pp. 1321–1330.
- [47] R. Müller, S. Kornblith, and G. E. Hinton, "When does label smoothing help?" in *Advances in Neural Information Processing Systems 32, Vancouver, BC, Canada*, 2019, pp. 4696–4705.
- [48] D.-B. Wang, L. Feng, and M.-L. Zhang, "Rethinking calibration of deep neural networks: Do not be afraid of overconfidence," in *Advances in Neural Information Processing Systems 34, Virtual Event*, 2021, pp. 11 809–11 820.
- [49] S. Thulasidasan, G. Chennupati, J. A. Bilmes, T. Bhattacharya, and S. Michalak, "On mixup training: Improved calibration and predictive uncertainty for deep neural networks," in *Advances in Neural Information Processing Systems 32, Vancouver, BC, Canada*, 2019, pp. 13 888–13 899.
- [50] L. Zhang, Z. Deng, K. Kawaguchi, and J. Zou, "When and how mixup improves calibration," in *Proceedings of the 39th International Conference on Machine Learning, Baltimore, Maryland, USA*, vol. 162, 2022, pp. 26 135–26 160.
- [51] J. Mukhoti, V. Kulharia, A. Sanyal, S. Golodetz, P. H. S. Torr, and P. K. Dokania, "Calibrating deep neural networks using focal loss," in *Advances in Neural Information Processing Systems 33, Virtual Event*, 2020, pp. 15 288–15 299.
- [52] L. Tao, M. Dong, and C. Xu, "Dual focal loss for calibration," in *Proceedings of the 40th International Conference on Machine Learning, Honolulu, HI, USA*, 2023, pp. 33 833–33 849.
- [53] J. Platt *et al.*, "Probabilistic outputs for support vector machines and comparisons to regularized likelihood methods," *Advances in Large Margin Classifiers*, vol. 10, no. 3, pp. 61–74, 1999.
- [54] C. Tomani, S. Gruber, M. E. Erdem, D. Cremers, and F. Buettnner, "Post-hoc uncertainty calibration for domain drift scenarios," in *Proceedings of the 32th IEEE/CVF Conference on Computer Vision and Pattern Recognition, Virtual Event, June 19–25, 2021, 2021*, pp. 10 124–10 132.
- [55] D.-B. Wang, L. Li, P. Zhao, P.-A. Heng, and M.-L. Zhang, "On the pitfall of mixup for uncertainty calibration," in *Proceedings of the 34th IEEE/CVF Conference on Computer Vision and Pattern Recognition, Vancouver, BC, Canada*, 2023, pp. 7609–7618.
- [56] D.-B. Wang and M.-L. Zhang, "Calibration bottleneck: Over-compressed representations are less calibratable," in *Proceedings of the 41st International Conference on Machine Learning, Vienna, Austria*, 2024, pp. 52 156–52 170.
- [57] T. Lin, P. Goyal, R. B. Girshick, K. He, and P. Dollár, "Focal loss for dense object detection," *IEEE transactions on pattern analysis and machine intelligence*, no. 2, pp. 318–327, 2020.
- [58] Y. LeCun, L. Bottou, Y. Bengio, and P. Haffner, "Gradient-based learning applied to document recognition," *Proceedings of the IEEE*, vol. 86, no. 11, pp. 2278–2324, 1998.
- [59] H. Xiao, K. Rasul, and R. Vollgraf, "Fashion-MNIST: A novel image dataset for benchmarking machine learning algorithms," *CoRR*, vol. abs/1708.07747, 2017. [Online]. Available: <http://arxiv.org/abs/1708.07747>
- [60] B. Settles, M. Craven, and S. Ray, "Multiple-instance active learning," in *Advances in Neural Information Processing Systems 20, Vancouver, British Columbia, Canada*, 2007, pp. 1289–1296.

APPENDIX A

PROOF OF LOWER BOUND AND REGULARIZATION PROPERTIES OF CDL (THEOREM 1)

Theorem 1 (Lower Bound and Regularization Properties of CDL). *Let \mathcal{L}_{CDL} denote the Calibratable Disambiguation Loss and \mathcal{L}_{MDL} denote the Momentum-based Disambiguation Loss. For any multi-instance bag \mathbf{X}_i with the candidate label set \mathcal{S}_i , under the condition that $\Phi(\hat{\mathbf{p}}_i^{(t)}) \in [\max_{c' \in \mathcal{S}_i} \hat{p}_{i,c'}^{(t)} - 1, \max_{c' \in \mathcal{S}_i} \hat{p}_{i,c'}^{(t)}]$, the following inequality holds:*

$$\mathcal{L}_{CDL} \geq (1 - \gamma\beta_i)\mathcal{L}_{MDL} = (1 - \gamma\beta_i)(\text{KL}(w_i \parallel \hat{p}_i) + \mathbb{H}[w_i]), \quad (\text{A1})$$

where $\beta_i = \max_{c' \in \mathcal{S}_i} \hat{p}_{i,c'}^{(t)} - \Phi(\hat{\mathbf{p}}_i^{(t)})$ represents the confidence margin of the multi-instance bag \mathbf{X}_i , $\gamma \in [1, \frac{1}{\beta_{\max}})$ controls the regularization strength, and $\beta_{\max} = \max_i \beta_i$ is the maximum confidence margin across all multi-instance bags in the dataset.

Proof. We begin with the definition of CDL, simplifying notation by omitting the superscript (t) for clarity. The loss function is expressed as follows:

$$\mathcal{L}_{CDL} = - \sum_{c \in \mathcal{S}_i} w_{i,c} (1 - \max_{c' \in \mathcal{S}_i} \hat{p}_{i,c'} + \Phi(\hat{\mathbf{p}}_i))^\gamma \log(\hat{p}_{i,c}). \quad (\text{A2})$$

Let us define an auxiliary function $\alpha_i(\hat{\mathbf{p}}_i)$ that encapsulates the scaling factor as follows:

$$\alpha_i(\hat{\mathbf{p}}_i) = 1 - \max_{c' \in \mathcal{S}_i} \hat{p}_{i,c'} + \Phi(\hat{\mathbf{p}}_i). \quad (\text{A3})$$

For the regularization term to be well-defined and mathematically sound, we impose the following constraint:

$$\Phi(\hat{\mathbf{p}}_i) \in [\max_{c' \in \mathcal{S}_i} \hat{p}_{i,c'} - 1, \max_{c' \in \mathcal{S}_i} \hat{p}_{i,c'}]. \quad (\text{A4})$$

This constraint ensures that $\alpha_i(\hat{\mathbf{p}}_i) \in [0, 1]$. For any integer $\gamma \geq 1$ and $\alpha_i(\hat{\mathbf{p}}_i) \in [0, 1]$, we can apply Bernoulli's inequality, stating that $(1 + x)^n \geq 1 + nx$ for any integer $n \geq 1$ and real number $x \geq -1$. By defining $x = \alpha_i(\hat{\mathbf{p}}_i) - 1$, where $x \geq -1$ since $\alpha_i(\hat{\mathbf{p}}_i) \geq 0$, we derive a lower bound for the loss function \mathcal{L}_{CDL} as follows:

$$\begin{aligned} \mathcal{L}_{CDL} &= - \sum_{c \in \mathcal{S}_i} w_{i,c} (\alpha_i(\hat{\mathbf{p}}_i))^\gamma \log(\hat{p}_{i,c}) \\ &\geq - \sum_{c \in \mathcal{S}_i} w_{i,c} [1 - \gamma(1 - \alpha_i(\hat{\mathbf{p}}_i))] \log(\hat{p}_{i,c}) \\ &= - \sum_{c \in \mathcal{S}_i} w_{i,c} \log(\hat{p}_{i,c}) \\ &\quad + \gamma \sum_{c \in \mathcal{S}_i} w_{i,c} (1 - \alpha_i(\hat{\mathbf{p}}_i)) \log(\hat{p}_{i,c}). \end{aligned} \quad (\text{A5})$$

The first term in Eq. (A5) corresponds to the momentum-based disambiguation loss (MDL), which can be written as:

$$\mathcal{L}_{MDL} = - \sum_{c \in \mathcal{S}_i} w_{i,c} \log(\hat{p}_{i,c}). \quad (\text{A6})$$

Since $\{w_{i,c}\}_{c \in \mathcal{S}_i}$ forms a valid probability distribution, i.e., $\sum_{c \in \mathcal{S}_i} w_{i,c} = 1$ and $w_{i,c} \geq 0$ for all $c \in \mathcal{S}_i$, we can express \mathcal{L}_{MDL} in terms of the Kullback-Leibler divergence and entropy as follows:

$$\mathcal{L}_{MDL} = \text{KL}(w_i \parallel \hat{p}_i) + \mathbb{H}[w_i], \quad (\text{A7})$$

where $\text{KL}(w_i \parallel \hat{p}_i) = \sum_{c \in \mathcal{S}_i} w_{i,c} \log \frac{w_{i,c}}{\hat{p}_{i,c}}$ represents the Kullback-Leibler divergence between the weighted distribution of the candidate labels w_i and the predicted distribution \hat{p}_i , and $\mathbb{H}[w_i] = -\sum_{c \in \mathcal{S}_i} w_{i,c} \log w_{i,c}$ denotes the entropy of the weighted distribution of the candidate labels.

For the second term in Eq. (A5), we expand $(1 - \alpha_i(\hat{p}_i))$ as $(\max_{c \in \mathcal{S}_i} \hat{p}_{i,c} - \Phi(\hat{p}_i))$ and derive the following:

$$\begin{aligned}
& \gamma \sum_{c \in \mathcal{S}_i} w_{i,c} (1 - \alpha_i(\hat{p}_i)) \log(\hat{p}_{i,c}) \\
&= \gamma \sum_{c \in \mathcal{S}_i} w_{i,c} (\max_{c' \in \mathcal{S}_i} \hat{p}_{i,c'} - \Phi(\hat{p}_i)) \log(\hat{p}_{i,c}) \\
&= \gamma (\max_{c' \in \mathcal{S}_i} \hat{p}_{i,c'} - \Phi(\hat{p}_i)) \sum_{c \in \mathcal{S}_i} w_{i,c} \log(\hat{p}_{i,c}) \\
&= -\gamma (\max_{c' \in \mathcal{S}_i} \hat{p}_{i,c'} - \Phi(\hat{p}_i)) \mathcal{L}_{\text{MDL}}.
\end{aligned} \tag{A8}$$

We define the confidence margin $\beta_i = \max_{c' \in \mathcal{S}_i} \hat{p}_{i,c'} - \Phi(\hat{p}_i)$. This allows us to rewrite our inequality in a more interpretable form as follows:

$$\begin{aligned}
\mathcal{L}_{\text{CDL}} &\geq \mathcal{L}_{\text{MDL}} - \gamma \cdot \beta_i \cdot \mathcal{L}_{\text{MDL}} \\
&= (1 - \gamma \beta_i) \mathcal{L}_{\text{MDL}} \\
&= (1 - \gamma \beta_i) (\text{KL}(w_i \parallel \hat{p}_i) + \mathbb{H}[w_i]).
\end{aligned} \tag{A9}$$

To ensure that this loss remains positive and stable across all multi-instance bags, the condition $\gamma \beta_i < 1$ must hold for each bag, which implies $\gamma < \frac{1}{\beta_{\max}}$, where $\beta_{\max} = \max_i \beta_i$ denotes the maximum confidence margin across the dataset. Additionally, Bernoulli's inequality imposes $\gamma \geq 1$, restricting the integer parameter γ to the range $[1, \frac{1}{\beta_{\max}})$. This derivation illustrates that \mathcal{L}_{CDL} is effectively a scaled version of the momentum-based disambiguation loss \mathcal{L}_{MDL} , with the scaling factor $(1 - \gamma \beta_i)$ determined by both the regularization parameter γ and the confidence margin β_i . When $\Phi(\hat{p}_i)$ is carefully chosen, this scaling serves as an implicit regularization mechanism, mitigating overconfidence in the model's predictions by adjusting the influence of \mathcal{L}_{MDL} based on the confidence margin.

This completes the proof of Theorem 1. \square